İZMİR KÂTİP ÇELEBİ ÜNİVERSİTESİ
2010
GRADUATE SCHOOL OF NATURAL AND APPLIED SCIENCES

Controlling the Motion of Capillary Driven Interfaces in Channels with Chemical Heterogeneity

Submitted to the Graduate School of Natural and Applied Sciences in partial fulfillment of the requirements for the degree of

Master of Science

in Mechanical Engineering

by

Mehmet Alptuğ Boylu

ORCID 0000-0003-1856-7606

February, 2023

This is to certify that we have read the thesis **Controlling the Motion of Capillary Driven Interfaces in Channels with Chemical Heterogeneity** submitted by **Mehmet Alptuğ Boylu**, and it has been judged to be successful, in scope and in quality, at the defense exam and accepted by our jury as a MASTER'S THESIS.

APPROVED BY:

Advisor: **Asst. Prof. Dr. Umut Ceyhan**
İzmir Kâtip Çelebi University

Committee Members:

Assoc. Prof. Dr. Mehmet Akif Ezan
Dokuz Eylul University

Assoc. Prof. Dr. Utku Şentürk
Ege University

Date of Defense: February 2, 2023

Declaration of Authorship

I, **Mehmet Alptuğ Boylu**, declare that this thesis titled **Controlling the Motion of Capillary Driven Interfaces in Channels with Chemical Heterogeneity** and the work presented in it are my own. I confirm that:

- This work was done wholly or mainly while in candidature for the Master's degree at this university.
- Where any part of this thesis has previously been submitted for a degree or any other qualification at this university or any other institution, this has been clearly stated.
- Where I have consulted the published work of others, this is always clearly attributed.
- Where I have quoted from the work of others, the source is always given. This thesis is entirely my own work, with the exception of such quotations.
- I have acknowledged all major sources of assistance.
- Where the thesis is based on work done by myself jointly with others, I have made clear exactly what was done by others and what I have contributed myself.

Signature:

_____

Date: 02.02.2023

_____

Controlling the Motion of Capillary Driven Interfaces in Channels with Chemical Heterogeneity

Abstract

The use of self-driven fluids (e.g., droplets, capillary flows) attracts many researchers as the external driving mechanisms are diminished or eliminated. The contact angle hysteresis generates a driving force (a pressure difference across interfaces). This pressure depends on the interaction with the solid substrates and is controlled if one varies the surface energy of the walls. Self-transport and manipulation of interfaces play an important role in the development of microfluidic devices, self-cleaning, water harvesting and heat transfer enhancement. In this study, we search for the effects of surface energy on the motion of interfaces. To this end, we model the motion of fluid particles and integrate the governing equations using the D2Q9 binary lattice Boltzmann method for the two-phase flow. We, first, validate our solver for canonical static and dynamic problems. We, then, discuss two main contributions; The first one is, for capillary driven flows, we show how to deviate the interface speed from the ones moving in channels with uniform wall energies, the conditions under which the interface stagnates (like a passive valve in a channel). Tuning the wettability of the channel walls, we provide a simple criteria for stopping the interface: the summation of the equilibrium contact angles interface make with the channel walls at the bottom and top wall need to satisfy $\theta_{eq}^{bot} + \theta_{eq}^{top} \geq \pi$. The second contribution is that, by varying the surface energy and fluid viscosities, we systematically study the behavior of single droplets on surfaces, their merging mechanism and equilibrium shapes and motions within confinements.

Keywords: Capillarity, Wetting, Interface, Microfluidics, Lattice Boltzmann Method, Interfacial Flow, Contact Lines, Wettability Gradient

Kanal İçerisindeki Kapilerite ile İlerleyen Arayüzlerin Kimyasal Heterojen Yüzeyler ile Kontrolü

Öz

Harici tahrik mekanizmaları azaldığından veya ortadan kalktığından, kendi kendine hareket eden sıvıların (örn. damlacıklar, kılcal akışlar) kullanımı birçok araştırmacının ilgisini çekmektedir. Temas açısı histerezisi, bir itici güç (arayüzler arasında bir basınç farkı) üretir. Bu basınç, katı yüzeylerle etkileşime bağlıdır ve duvarların yüzey enerjisi değiştirilerek kontrol edilir. Arabirimlerin kendi kendine taşınması ve manipülasyonu, mikroakışkan cihazların geliştirilmesinde, kendi kendini temizlemede, su toplamada ve ısı transferinin geliştirilmesinde önemli bir rol oynar. Bu çalışmada, yüzey enerjisinin arayüzlerin hareketi üzerindeki etkilerini araştırıyoruz. Bu amaçla, sıvı parçacıklarının hareketini modelliyoruz ve iki fazlı akış için D2Q9 ikili kafes Boltzmann yöntemini kullanarak, yöneten denklemleri entegre ediyoruz. Öncelikle standart statik ve dinamik problemler için çözücümüzü doğrularız. Daha sonra, iki ana katkıyı tartışıyoruz; Bunlardan birincisi, kılcal tahrikli akışlar için, arayüz hızının, değişmeyen duvar enerjilerine sahip kanallarda hareket edenlerden nasıl saptırılacağını ve böyle bir arayüzün hangi koşullar altında durduğunu (bir kanaldaki pasif bir valf gibi) gösteriyoruz. Kanal duvarlarının ıslanabilirliğini ayarlayarak arayüzü durdurmak için basit bir kriter sağlıyoruz: arayüzün alt ve üst duvardaki kanal duvarlarıyla yaptığı denge temas açılarının toplamı $\theta_{eq}^{bot} + \theta_{eq}^{top} \geq \pi$ 'yi sağlamalıdır. İkinci katkı ise, yüzey enerjisini ve sıvı viskozitelerini değiştirerek, tek damlacıkların yüzeyler üzerindeki davranışını, bunların birleştirme mekanizmasını ve sınırlamalar içindeki denge şekillerini ve hareketlerini sistematik olarak inceliyoruz.

Anahtar Kelimeler: Kapilarite, Islatma, Arayüzey, Mikroakışkanlar, Lattice Boltzmann Metodu, Arayüzey Akışı, Kontakt Çizgileri, Islanabilirlik Gradyanı

To my beloved ones.

Acknowledgment

I would like to express my deepest gratitude to my advisor, Umut Ceyhan, for their invaluable guidance, support, and encouragement throughout the course of this thesis.

I am also grateful to the rest of my thesis committee, Mehmet Akif Ezan and Utku Şentürk, for their valuable feedback and insights.

Finally, I would like to thank my family and friends for their unwavering support and encouragement. This work would not have been possible without their love and belief in me.

Table of Contents

List of Figures

List of Tables

List of Abbreviations

BGK	Bhatnagar–Gross–Krook
CAH	Contact Angle Hysteresis
CFD	Computational Fluid Dynamics
DWC	Dropwise Condensation
FWC	Filmwise Condensation
LBM	Lattice Boltzmann Method
MRT	Multiple Relaxation Time

List of Symbols

a	Constant coefficient in Landau model
Ca	Capillary number ($\eta v/\gamma$)
ε	Parameter for wetting property
η	Dynamic viscosity
F_i	Body (external) force
f_i	Distribution function f
g_i	Distribution function g
γ	Surface tension between fluids
Γ	Constant of mobility
h	Channel gap thickness
κ	Coefficient in Landau model
l	Capillary filling length
λ	Viscosity ratio of fluids
M	Mobility
μ	Chemical potential
$\boldsymbol{n}$	Outward unit normal
n_x	Number of lattices along x-axis
n_y	Number of lattices along y-axis
$\emptyset$	Order parameter (phase field)
$P_{\alpha\beta}$	Pressure tensor
p_g	Gas pressure
p_l	Liquid pressure

r	Radius of curvature
ρ	Density
S	Bounding surface of the corresponding ϑ
t	Time
τ_α	Relaxation time parameter for fluid 1
τ_β	Relaxation time parameter for fluid 2
θ	Contact angle
θ_{eq}	Equilibrium contact angle
v	Velocity
ν_g	Kinematic viscosity of gas
ν_l	Kinematic viscosity of liquid
ϑ	Volume

Chapter 1

Introduction

The experimental and theoretical studies of self-driven droplets and flows have made major strides in recent years. But there are still lots of unanswered concerns and a lot to learn about these systems. The potential for self-driven droplets and the flows to produce significant insights and developments makes this an interesting and popular area of research. The physics of fluids on micron-scale is affected by the surface energy of the interfaces, here, the strong interaction between the fluid and solid substrate [1,2]. The motion of the contact line where the liquid meets the solid surface is dominated by viscous and surface tension forces rather than inertial and gravitational forces [3,4]. The ratio of the two forces is the Capillary number. The motion of the interface is driven only by the pressure difference across the liquid interface. Any variation in the chemical structure of the surface over which the contact line moves, changes the dynamics of the contact line motion. For example, in heat transfer on the surfaces, manipulation of droplets by wetting gradients are promising to increase the efficiency of heat transfer. Occurrence of condensation either as filmwise condensation (FWC) or dropwise condensation (DWC) affects the mechanism of heat transfer. As continuous film creates a resistance for heat transfer, dropwise condensation is more effective. But in high rates of temperature differences (degree of subcooling), it cannot be possible to observe DWC [5,6].

Surface tension must be taken into account while doing a research of self-driven droplets and flows since it is a major factor in influencing the form and stability. When an interface meets a solid surface, it makes a certain angle with the interface which is called contact angle. This angle depends on the nature of the solid surface and the history of how the interface is established. To help with the remaining of the thesis, we start with some basic definitions like wetting and contact angle hysteresis.

Wetting, which is defined as a liquid's capacity to stick to a solid surface, is an important factor of many natural and industrial processes. There are so many applications that require the liquid spreading on solid substrates (solid substrate could be a homogeneous surface or like a porous surface). There are types of wetting according to that amount of the sticking capacity. In terms of types, the notion of "wetting transition" which is used to explain how liquids behave on solid surfaces, was denoted by de Gennes in [7]. The "complete wetting" and "partial wetting" systems are shown in Figure 1.1.

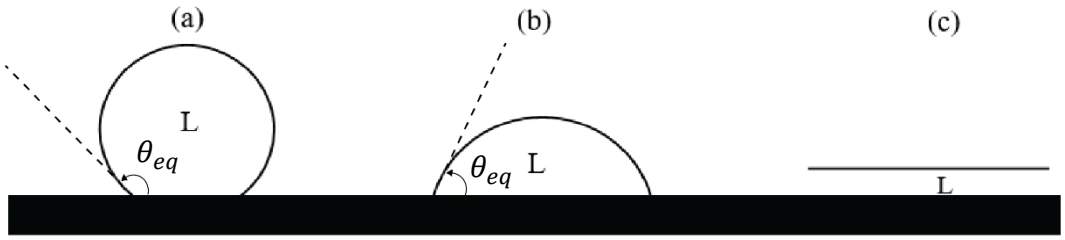

Figure 1.1: Liquids on a solid substrate, (a) hydrophobic ($180° > \theta_{eq} > 90°$) and (b) hydrophilic ($\theta_{eq} < 90°$) systems show the partial wetting; the wetting is stronger in (b) than (a), (c) shows the complete wetting ($\theta_{eq} = 0°$).

The ability of a liquid to wet a solid surface is called as wettability, and it is affected by the relative energies of the liquid-solid and liquid-vapor interfaces. If the liquid-vapor interface energy is greater than the liquid-solid interface energy, we can say the surface is hydrophobic, but if the liquid-solid interface energy is greater than the liquid-vapor interface energy, then we can define the surface as hydrophilic (water attracting).

For atomically smooth and chemically homogeneous surfaces, this angle is unique [8]. However, in nature, there are always heterogeneities or the surface can be designed as heterogeneous on purpose [9]. In this case, the contact angle is not unique; there is contact angle hysteresis (CAH) [10-12]. The heterogeneities, either physical or chemical, may cause contact line pinning/depinning. Many natural and engineering processes, including capillary action, adhesion, and friction depend on wettability. Surface chemistry, surface roughness, temperature, pressure, and the characteristics of the liquid and the solid parameters, all of them can affect the wettability. In this thesis, we mainly interest in the surface chemistry.

The phenomenon known as contact angle hysteresis (CAH) can be seen when the contact angle between a liquid droplet and a solid surface changes according to the direction in which the droplet is moving. The larger contact angle at the droplet's front is called the "advancing contact angle," and the smaller contact angle at the back or tail of the droplet is called the "receding contact angle." The "hysteresis loop" is a measure of the "wetting behavior" of the liquid on the solid substrate and this is known as the difference between the advancing and receding contact angles. In systems where the solid's surface energy varies or when the surface is chemically or mechanically heterogeneous, contact angle hysteresis can be seen more often.

The contact angle hysteresis can also be affected by parameters such as droplet size, droplet velocity, and the impurities in the liquid or on the solid surface. In materials science, chemistry, and engineering, understanding and controlling the contact angle hysteresis is more important in terms of the functionality of processes that depend on wetting behavior.

Because the spreading droplets over rough substrates and evaporation/condensation of droplets cause a natural motion of interfaces, the CAH over heterogeneous surfaces for such interfaces takes the great attention of many researchers [13-15]. The droplet may attain an equilibrium shape, pin(depin) to(from) structures, move due to hysteresis. For example, if the surface is more wetting (more prone to spreading out) at one end than at the other, the droplet tries to move towards the more wetting end. This happens because the liquid spreads more and make a larger contact area with the solid substrate at the more wetting end, which can cause the droplet to be pulled towards that direction due to capillary forces [1, 16-20]. In other words, the droplet moves from low-surface energy side towards the high-energy side. It is known that self-transport is faster for low-surface tension fluids like ethanol compared to water as it is more wetting [21,22] on fixed substrate. But without altering the surface tension of the droplet, its shape or motion can be controlled by varying the surface energy of the surfaces [23]. Geometric gradients like self-motion of droplets on conical surfaces is also possible (see, e.g., Ding et al 2023 [24]). Assisted by both surface gradients and wetting gradients, a droplet may further be accelerated. The capillaries also provide such motion for the interfaces. For a liquid filling a capillary, the motion of the interface is driven only by the pressure

difference across the liquid interface. With the advancement in the understanding of wetting phenomena, its use in microfluidic devices has been increasing.

Interface motion in capillary driven flows and wetting phenomena on heterogeneous substrates (e.g., self-transport and manipulation of droplets) are observed in nature [25,26], mostly in plants-trees [27], lotus leaves [28], desert beetles [29] and butterfly wings [30] etc.; and in engineering applications such as lab-on-chips [31-34], heat transfer enhancement [35,36], self-cleaning [37], oil recovery [38], painting, and inkjet printing [39-41]. Understanding and controlling the motion of such interfaces are important in microfluidic devices. Generally, the interfaces are controlled with active methods (actuators, valves), which require labor and are not scalable, autonomous, and easy to adapt and implement [42,43]. We, instead, investigate the use of different wettability regions, e.g., provided by chemical heterogeneity in the control of interfaces passively which has plenty of advantages [44,45]. The idea of changing the wettability of surfaces and combining with liquid infusion or lubricant impregnation can be utilized, also, to vary the droplet speed, orientation, size etc. [46-50].

The lattice Boltzmann method is one of the numerical methods to be able to integrate the governing equations that control the motion of two-phase systems. Navier-Stokes, continuity and phase-field equations are modified into lattice Boltzmann equation with using Chapman Enskog expansion in the limit of long length and time scales [51]. This mesoscopic numerical method can be used for various types of problems, from simple fluids to complex chemical reactions. So, like the topological heterogeneities [52,53], similar effects are observable with chemical heterogeneities [8,54-56]. In this thesis, we use D2Q9 lattice Boltzmann method for simulating the problems because of the methods mobility for wetting problems and its lower computing cost due to its step-by-step solution (i.e., no requirement of matrix inversion), compared to traditional methods such as Finite Element, Finite Volume, Boundary Element Methods etc.

In the thesis' following sections, we begin by introducing the method that we use to simulate capillary problems. We summarize different implementations for the method as Bhatnagar–Gross–Krook (BGK), Multiple Relaxation Time (MRT) etc. [57]. After the methodology, we present validations of our solver for static (Young

equation) and dynamic (Washburn's and Cox-Voinov laws) problems. Later, we discuss the effect of chemical heterogeneity on the interface motion within capillaries and mechanism of self-driven single or multiple droplets on and within chemically structured surfaces.

Chapter 2

Model Problem

The problem setups for droplet and capillary interface cases are given in the figures 2.1 and 2.2 below. For both models, left-right ends are treated as periodic. For droplet modelling, top surface is away from the droplet. But for the confinement effect and capillary modelling, the top surface touches to the interface/s. The node number (lattices) change for different cases. The meadow green color shows the liquid as fluid 1(α) and the moss green color shows the gas as fluid 2(β).

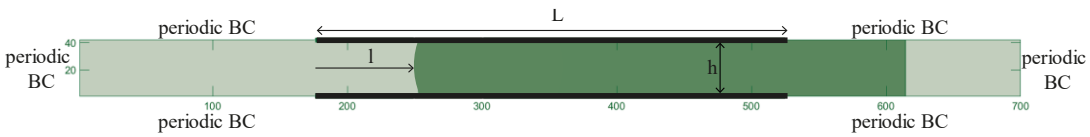

Figure 2.1: Capillary Model, wall length is L and filling length (l) is distance that liquid penetrates into the capillary tube. $n_x = 700$ and $n_y = 42$ lattices along x and y-directions, respectively; and capillary walls are placed in the middle of the domain at the top and bottom. For different viscosity cases we set the kinematic viscosities to $v_l = 0.83$ and $v_g = 0.067$ (this corresponds to $\tau_\alpha = 3$, $\tau_\beta = 0.7$ as in [58]).

The *L*-length channel walls for the capillary are shown in black. The periodic top and bottom sides give us a flat interface that mimics infinite reservoirs at both ends, while the periodic inlet and outflow bounds guarantee mass conservation. We set $\kappa = 0.04$, $a = 0.04$ and $M = 1$ in the lattice Boltzmann implementation with Multiple-Relaxation Time.

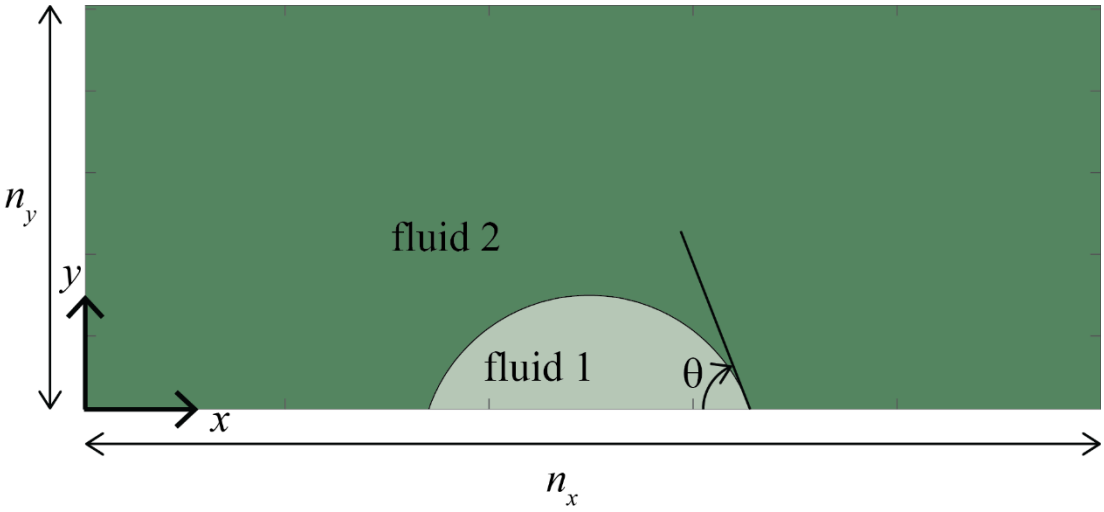

Figure 2.2: Droplet Model, n_x and n_y are the number of lattices used along x and y directions, time dependent contact angle $\theta(t)$ (according to problems) may be unique or different at both contact lines.

The problems we are interested in are affected greatly by the contact line dynamics. In Figure 2.2, we show our droplet model. Except the domain length and viscosity ratios, the same parameters within capillary model are used in this model. The wetting angle the contact lines make with the surfaces determine the statics and dynamics of the problem. To this end, we validate our solver for both static and dynamic problems.

2.1 Governing Equations

The Navier-Stokes equations of motion and the continuity for a Newtonian fluid, denoted by equations (2.1a) and (2.1b) in index notation, respectively, govern the motion of fluid particles inside the capillary in the continuum regime.

$$\partial_t(\rho v_i) + \partial_j\left(\rho v_j v_i\right) = -\partial_j P_{ji} + \partial_j\left(\eta\left(\partial_i v_j + \partial_j v_i\right)\right) + \rho F_i, \tag{2.1a}$$

$$\partial_t \rho + \partial_j\left(\rho v_j\right) = 0, \tag{2.1b}$$

where ρ is the density, η is the dynamic viscosity of the fluid, and v_j is the fluid velocity. In equations (2.1a) and (2.1b), the indices i, j vary from 1 to 2 in two-dimensional problem and twice appearing index j in an expression means summation over it. In right-hand side of the equation (2.1a), there are three terms: First term

includes the pressure tensor P_{ji} which is defined below (equation 2.2), second term is related with viscous forces and the last term defines the external body force per unit volume,

$$P_{ji} = \left(p_0 - \kappa\emptyset\nabla^2\emptyset - \frac{\kappa}{2}\left|\nabla\emptyset\right|^2\right)\delta_{ji} + \kappa\partial_j\emptyset\partial_i\emptyset. \tag{2.2}$$

There are pressure forces and surface tension forces inside the pressure tensor, and there is also an order parameter from the Landau Free Energy that will be defined shortly. Equation (2.2) gives the definition of the bulk pressure as

$$p_0 = \frac{c^3}{3}\rho + a\left(\frac{1}{2}\emptyset^2 + \frac{3}{4}\emptyset^4\right). \tag{2.3}$$

Interface profile and fluid motion are related with pressure as follows [59]. For non-uniform composition, $-\emptyset\nabla\mu$ models the surface tension forces which comes from the divergence of P_{ji}, moreover, it has a localized effect on the fluid (chemical potential creates the opposite motion of the two phases denoted by $\pm\emptyset$). $\emptyset$ controls the interface changes.

$$\emptyset\nabla\mu = \partial_j P_{ji}, \tag{2.4}$$

and the phase field is governed by Cahn-Hilliard type equation [60,61]

$$\partial_t\emptyset + \partial_j\left(\emptyset v_j\right) = M\nabla^2\mu. \tag{2.5}$$

M is referred to as mobility in equation (2.5), which regulates the strength of the diffusion. The phase field $\emptyset$ responds to gradients by diffusion (as seen on the right-hand side), and it also changes over time as a result of v_j's convection (as given on the left-hand-side).

2.2 Thermodynamics of the fluid: Modelling Free Energy

We use Landau theory to describe the binary fluids' free energy. It uses $\emptyset$ as a order parameter. First terms describe a second order phase transition in Landau function.

Landau free energy is defined as

$$F = \int \left(\varphi(\emptyset) + \frac{\kappa}{2}\left|\nabla\emptyset\right|^2\right) d\vartheta + \int (\varepsilon\emptyset) dS \tag{2.6}$$

where ϑ is the volume and S is the bounding surface of the corresponding volume, and the bulk free energy density $\varphi(\emptyset)$ is

$$\varphi(\emptyset) = \frac{c^2}{3}\rho\ln\rho + a\left(-\frac{1}{2}\emptyset^2 + \frac{1}{4}\emptyset^4\right). \tag{2.7}$$

We take ρ as a fluid density and $\emptyset$ is the order parameter $\emptyset = \pm 1$. c can be written as $\frac{\Delta x}{\Delta t}$ (Δx spacing between the points or lattices and Δt time step) and a is a constant. The κ term in equation (2.6) gives the interfaces with surface tension by penalizing non-uniformities (penalizes sharp gradients) in $\emptyset$. Surface tension between the phases is given by $\gamma_{lv} = \sqrt{8\kappa a/9}$ [62].

While the first terms describe a second-order phase transition in the Landau function, the second integral in equation (2.6) shows the solid-fluid interactions and models the surface tension between them. We control the contact angle with the ε parameter. For controlling the contact angle, we take partial derivative for $\emptyset$ at the boundary, with respect to the normal of the surface $\partial_\perp \emptyset|_w = \varepsilon/\kappa$.

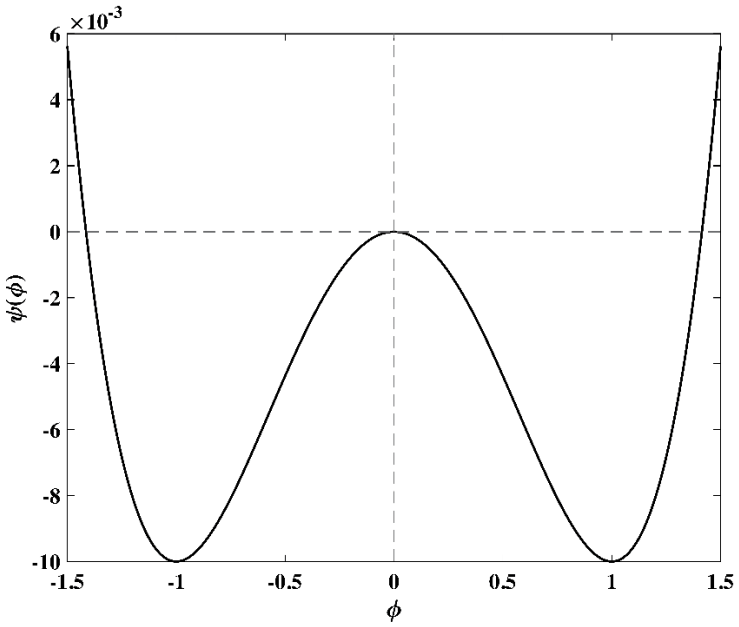

Figure 2.3: Phase separation, equilibrium values at $\pm\emptyset$.

We show the order parameter in Figure 2.3, the minimum points define the equilibrium state at fixed volume and temperature, equilibrium states are given by global minima of the free energy, F. The variation of equation (2.6) with respect to $\emptyset$ defines the chemical potential which is constant in equilibrium as

$$\mu = \frac{\delta F}{\delta \emptyset} = a(-\emptyset + \emptyset^3) - \kappa \nabla^2 \emptyset. \tag{2.8}$$

For the numerical solution of the governing equations, we use lattice Boltzmann Method. Applying Chapman-Enskog expansion [51] shows that the lattice Boltzmann method recovers the hydrodynamic (governing) equations.

Chapter 3

Numerical Method

3.1 Lattice Boltzmann Method

The discretization of the Boltzmann equation leads to the development of the Lattice Boltzmann method, a mesoscopic numerical integration approach for fluid dynamics. It describes how a gas or liquid behaves at this level. A particular lattice Boltzmann method known as the D2Q9 model uses a two-dimensional lattice with nine discrete velocity vectors and offers a wide range of fluid flow modeling.

By include a free energy functional in the Boltzmann equation, the D2Q9 model is able to represent thermodynamic variations in temperature and pressure. This functional can be used to calculate values like the equation of state, heat capacity, and surface tension $\gamma_{lv} = \sqrt{8\kappa a/9}$ [63] since it represents the system's total energy, which includes both kinetic and potential energy.

In order to add free energy into the D2Q9 model, we must first develop a set of distribution functions that express the possibility of coming along a particle with a specific velocity at a specific location in space and time. The Boltzmann equation is then used to evolve these distribution functions, which allows for particle collisions and interactions with the surrounding fluid.

Due to its ease of use and adaptability, the lattice Boltzmann method (LBM) has grown in popularity recently for computational fluid dynamics (CFD). The Boltzmann equation, which defines how the distribution function of a system of particles evolves, forms the basis for this thesis. This distribution function is

discretized on a lattice in LBM, and a series of discrete steps are used to mimic the particle dynamics. We use fixed nodes in LBM, there is no moving mesh.

The ability of LBM to simulate a variety of physical processes, such as fluid flow, heat transfer, and chemical reactions, is one of its key benefits. As it does not require the usage of explicit meshes, it is particularly well suited for issues involving complicated geometries and boundary conditions.

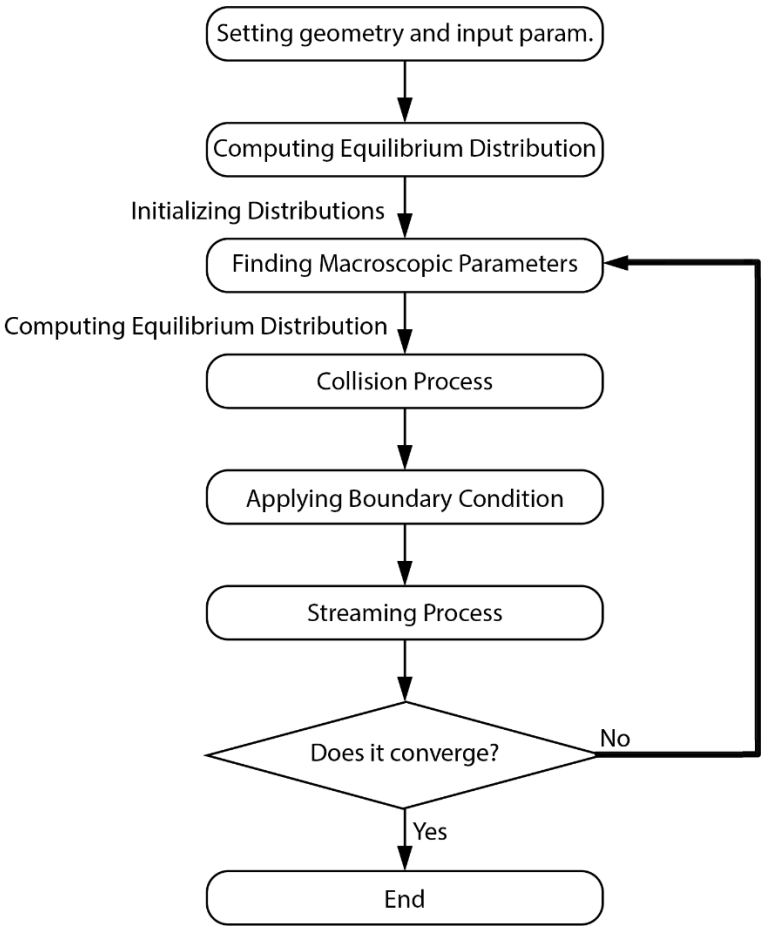

Figure 3.1: Implementation of LBM Flow-chart

A set of discrete velocities and a lattice structure must first be defined in order to implement LBM. After initializing the distribution function, the system is evolved using the steps as shown in Figure 3.1:

1. Macroscopic variables: The macroscopic variables (e.g., density, velocity) are computed from the distribution function.
2. Collision: A collision operator, which simulates the interactions between particles and the surface forces, is used to transform the distribution function.
3. Boundary conditions: To adjust for any external forces or system constraints, the distribution function is modified.
4. Streaming: Depending on their velocities, the particles are transferred from one lattice site to another.

Until the system reaches a steady state or the desired simulation period has ended, these stages are repeated.

3.1.1 Macroscopic Variables

All dimensions are given in lattice units. As we analyse the physical behaviour of interfaces for a binary fluid system, we use two distribution functions as $f_i(r,t)$ and $g_i(r,t)$. The subscript i shows the directions defined in a vector e_i, that the lattice point can travel. The values are as follows: $e_0 = (0,0), e_1 = (+c,0)$, $e_2 = (-c,0)$, $e_3 = (0,+c)$, $e_4 = (0,-c)$, $e_5 = (+c,+c)$, $e_6 = (-c,-c)$, $e_7 = (-c,+c)$, $e_8 = (+c,-c)$ and the illustration of the directions is given in Figure 3.2.

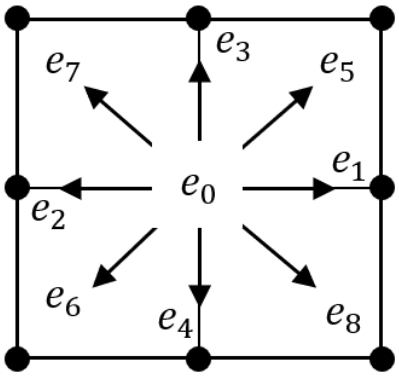

Figure 3.2: The subscript i shows the directions defined in a vector e_i , that the lattice point can travel.

The physical quantities can be constructed from the distribution functions by

$$\rho = \sum_i f_i \, , \emptyset = \sum_i g_i \, , \rho v = \sum_i f_i e_i . \tag{3.1a}$$

In LBM, we separate the collision equation (3.1b-3.1c) and streaming equation (3.1d-3.1e) operations [64] as given by

$$f_i'(r,t) = f_i(r,t) - inv[M]\left(S\left(M\left[f_i - f_i^{eq}\right]\right)\right), \tag{3.1b}$$

$$g_i'(r,t) = g_i(r,t) - \frac{1}{\tau_\emptyset}\left[g_i - g_i^{eq}\right], \tag{3.1c}$$

$$f_i(r + e_i\Delta t, t + \Delta t) = f_i'(r,t), \tag{3.1d}$$

$$g_i(r + e_i\Delta t, t + \Delta t) = g_i'(r,t). \tag{3.1e}$$

3.1.2 Relaxation Parameters

For the collision part, there is a collision operator parameter which includes a time constant τ as "relaxation time" parameter and describes the speed of the system to reach its equilibrium. The viscosity and heat diffusivity are affected by the relaxation time. Actually, Boltzmann's original collision operator is a non-trivial. It includes all the possibilities for a collision of two-particles. However, there is a simple operator that directly captures the relaxation of the distribution function with using single relaxation time (SRT) τ, to its equilibrium. Bhatnagar, Gross and Krook (BGK) collision operator [65] is given by

$$\Omega(f) = -\frac{1}{\tau}(f - f^{eq}). \tag{3.2}$$

Though the BGK operator is simple and efficient, it has lower accuracy and stability problems compared to Two-Relaxation-Time and Multiple-Relaxation-Time operators. We implement Multiple-Relaxation-Time (MRT) operator because it consists of more than two free parameters (relaxation times) to be arranged for more

stable and accurate results. In the BGK operator, we define only one relaxation parameter for the Boltzmann equation; but, in the multiple relaxation time, we define multiple relaxation parameter inside S matrix; M matrix and its inverse [63].

The equilibrium distribution functions can be shown as f_i^{eq} and g_i^{eq}. The relations between f_i and g_i is provided with f_i^{eq} and g_i^{eq}. We choose the equilibrium functions and gradients in a way to reduce spurious velocities around the interfaces [58].

The relaxation parameters seen in equation (3.1c) and in matrix S (equation 3.1b) are τ_ρ and $\tau_\emptyset$. While the $\tau_\emptyset$ is fixed and unity, τ_ρ varies from one lattice node to another by

$$\tau_\rho = \tau_\beta + \frac{\emptyset + 1}{2}(\tau_\alpha - \tau_\beta), \tag{3.3}$$

where τ_α and τ_β are the relaxation parameters that describe the fluids' viscosities. These relaxation parameters are related to the kinematic viscosity and mobility as

$$\nu = \Delta t \frac{c^2}{3}(\tau_\rho - \frac{1}{2}), \tag{3.4a}$$

$$M = \Delta t \Gamma (\tau_\emptyset - \frac{1}{2}), \tag{3.4b}$$

where Γ is a parameter that we set in the equilibrium to change mobility [58].

3.1.3 Push-Pull Penetrations

The terms "push" and "pull" in the LBM relate to two various methods of updating the distribution function, which expresses the probability density of particles filling various states on a lattice.

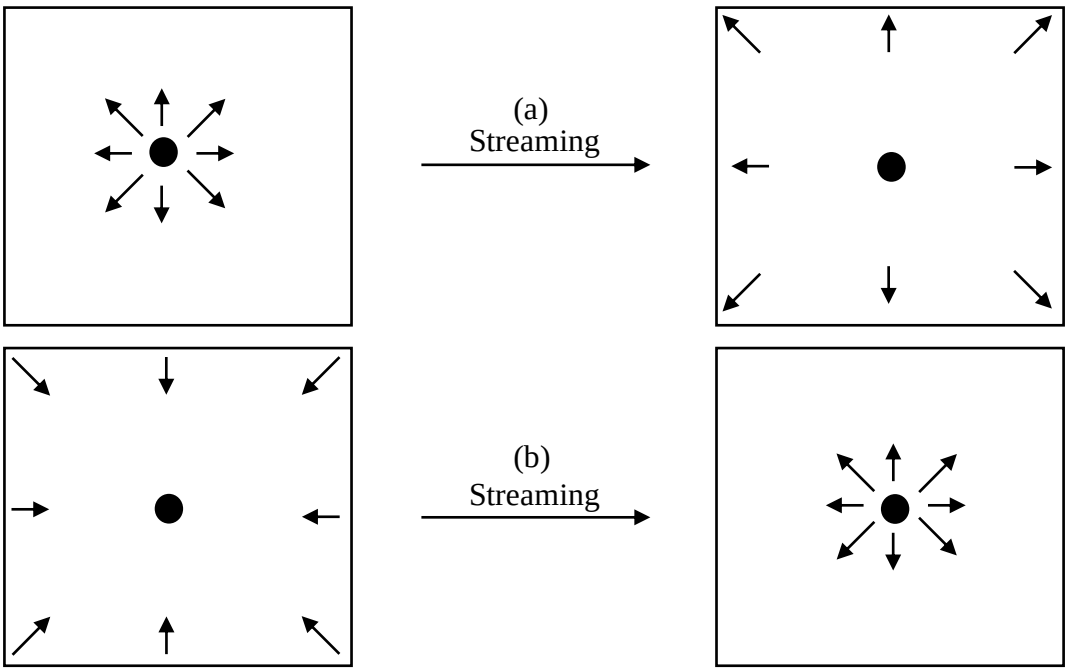

Figure 3.3: (a) Push propagation, (b) Pull propogation

By streaming the particles from their existing lattice sites to new sites in accordance with a set of discrete velocities, the "push" approach modifies the distribution function shown in Figure 3.3(a). Following the streaming process, the particles interact in collisions with one another and with any outside forces. The distribution function is updated during the collision step, and it is checked to see if the local equilibrium requirement is met.

A different approach to update the distribution function that is created to increase the stability of the LBM is the "pull" method as illustrated in Figure 3.3(b). The distribution function is changed twice in the pull technique. The particles are pushed to new locations in the first stage, but their velocities are not changed. To make sure that the distribution function meets the local equilibrium requirement, the velocities are updated in the second step.

Generally, the pull method is more difficult and memory-intensive than the push method, but it has the potential to be more stable, particularly when the Reynolds number is large.

3.1.4 Boundary Conditions

The boundary conditions are a key factor in determining how the system behaves at the domain's boundaries in the LBM. The no-slip boundary condition, which specifies that the fluid velocity is equal to zero at the solid walls of the domain, is the boundary condition that is most frequently utilized in LBM.

The midway bounce-back technique is one approach for LBM implementation of no-slip boundary requirements. This method effectively cancels out the effects of the particles that have opposing directions at the boundary by having particles that arrive at a boundary node during the streaming step to be reflected back to their original positions with the opposite velocities.

Both the "push" and "pull" variations of LBM can be solved using the halfway bounce-back technique. In the push technique, for instance, a particle is reflected back when it encounters a boundary node during the streaming stage, and the related distribution function is changed with a negative weight. The second step of the pull technique has no effect on the particles that are reflected at the boundaries, and the velocities of the reflected particles are not updated in the pull method.

It's important to note that this method requires the solid wall to be represented as a separate lattice, is inapplicable to curved or irregular boundaries, and may introduce errors at the boundary layer. Depending on the issue or level of accuracy desired, other more advanced boundary conditions methods like "Zou He" [66] etc. are also available.

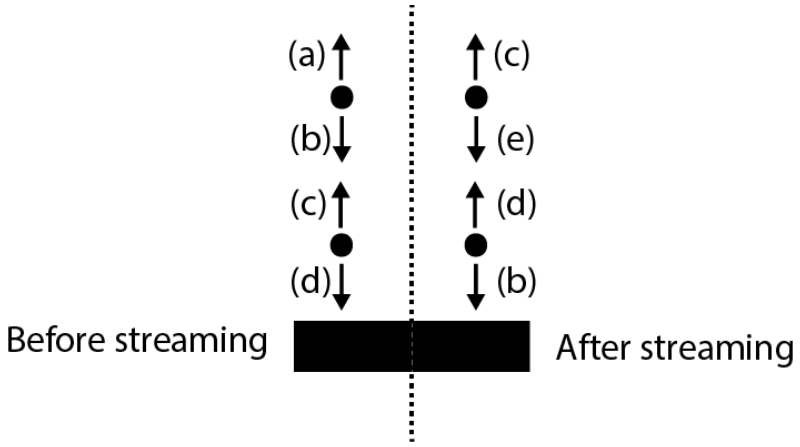

Figure 3.4: Illustration of implementing the boundary condition

In this thesis, halfway bounce-back method [67] ($f_i(x_N, t + \Delta t) = f^*_{opp(i)}(x_N, t)$) is used to apply no-slip boundary condition on the walls as seen in Figure 3.4.

Chapter 4

Interfaces with Chemically Homogeneous Surfaces: Validation

We devote this section to interfaces meeting chemically homogeneous surfaces for validation purposes. The capability of our solver for an interface to attain the correct equilibrium angle (static and dynamic angle) is crucial for the moving interfaces. We, first, validate our solver for static wetting problems on chemically homogeneous substrates for different surface energies. We measure the contact angles of certain droplet-substrate combinations to compare with the Young value. Second, we analyse the motion of interfaces within a capillary.

4.1 Static Validation

When a droplet meets a clean surface and remains in hydrostatic equilibrium, the contact angle it makes with the surface is given by the Young [68] value as

$$\cos\theta_{eq} = \frac{\gamma_{sv} - \gamma_{sl}}{\gamma_{lv}}, \tag{4.1}$$

where γ_{sv}, γ_{sl} and γ_{lv} are the surface tensions between solid-vapor, solid-liquid and liquid-vapor interfaces, respectively.

For a given liquid with fixed γ_{lv}, we vary the surface energy by tuning the normal gradient of $\emptyset$ at the boundary and setting the equilibrium contact angle given by equation (4.2)

$$\sqrt{\frac{2\kappa}{a}}\partial_{\perp}\emptyset|_{w} = 2\mathrm{sgn}\left(\theta_{eq} - \frac{\pi}{2}\right) \times \left[\cos\left(\frac{\Theta}{3}\right)\left(1 - \cos\left(\frac{\Theta}{3}\right)\right)\right]^{\frac{1}{2}}, \tag{4.2}$$

where $\Theta = \arccos\left((\sin\theta_{eq})^2\right)$ [62].

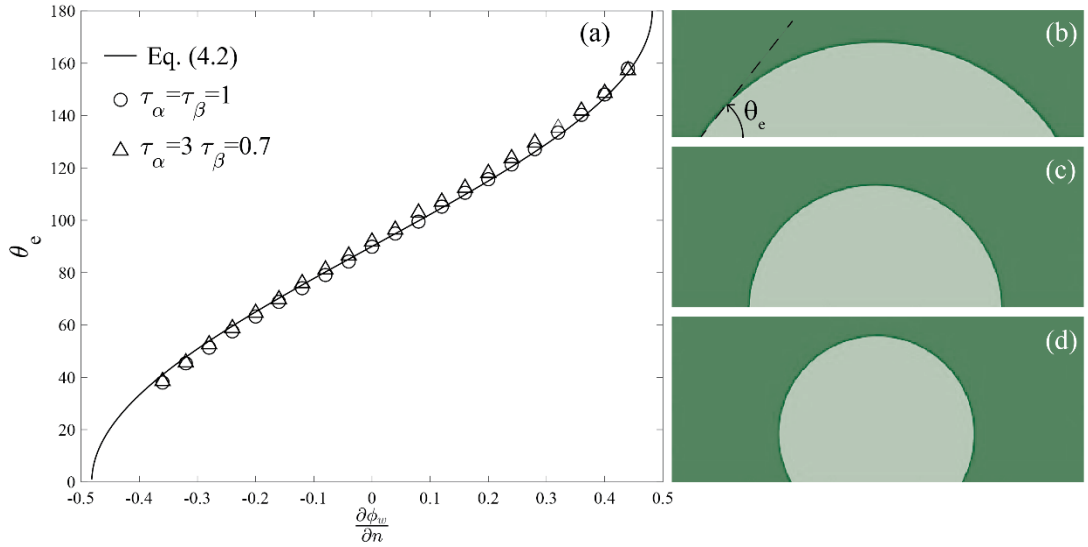

Figure 4.1: (a) The variation of equilibrium contact angle with gradient of $\emptyset$ at the wall $\partial_{\perp}\emptyset|_{w}$, for the same and different viscosities, respectively. Circles and triangles are simulation results obtained using MRT lattice Boltzmann. We show the theoretical expression given in equation (4.2) with a solid line. (b), (c) and (d) shows the equilibrium shapes of the droplets with $60°, 90°$ and $120°$ respectively.

We place a droplet on a flat, atomically smooth, and chemically uniform substrate. The droplets are not exposed to any external forces, and the surface tension is assumed to be uniform. We allow the droplets to converge to their equilibrium shape after initializing them as semicircles. The contact angle is time dependent and variation of it is given in Figure 4.2(a). In Figure 4.1(a), we compare the computed equilibrium contact angles with equation (4.2) and show the interface profiles for both partial wetting and non-wetting cases through in Figure 4.1(b)-(d). For the $60°$ equilibrium angle droplet spreading illustration by time are also given in 4.2 as in one panel (b). We perform the contact angle measurement by fitting a circle to the interface which is defined at the transition of $\emptyset$ from -1 to 1. The theory and computation match for the range of contact angles studied using MRT lattice Boltzmann method for both equal and different viscosity fluids. Using BGK instead

of MRT ends up with a deviation from the theory for different viscosities. A similar observation can be seen in Pooley et al. [63].

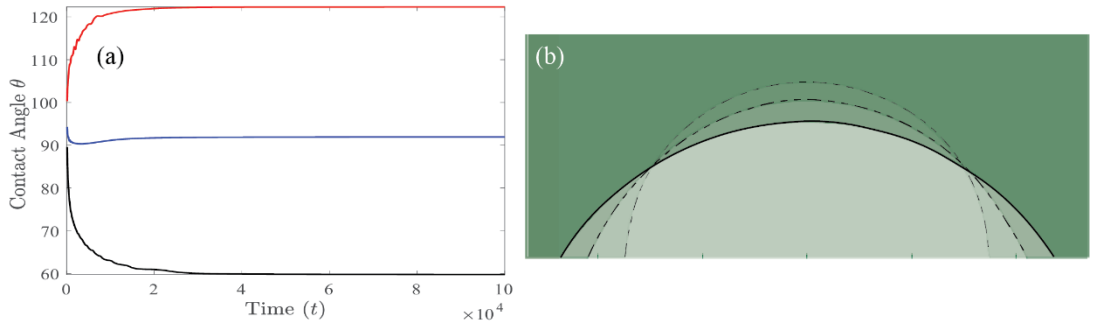

Figure 4.2: There are 3 cases as seen in Figure 4.1 (b),(c) and (d). In panel (a), the contact angle variations with respect to time are given. In panel (b), the evolution of the interface starting from a semi-circle to the one satisfying an equilibrium angle of 60° is given.

We also measure the pressure difference across the interface at equilibrium and validate $p_d - p_o \sim \gamma/r$ where p_d is the pressure inside the droplet, p_o is the outside pressure, γ is the surface tension between droplet and outside fluid and r^{-1} is the radius of curvature of the droplet interface.

4.2 Dynamic Validation

Capillary filling is one of the examples of moving contact line problems due to pressure difference across the moving interface. Because the motion does not require an external driving mechanism, it is one of the promising methods used in microfluidics. Washburn [69] defines the filling of a smooth capillary with constant surface energy. By neglecting the inertial effects, end effects and viscous effects due to displaced fluid (e.g., gas) by the filling liquid, the motion of the penetrating incompressible liquid is defined by Poiseuille flow. The position of the interface as function of time can be shown to obey the following power law relation

$$z(t)^2 - z_0^2 = l(t)^2 = \left(\frac{\gamma_{lv} h \cos\theta(t)}{3\eta}\right) t, \tag{4.3}$$

with $z(t=0)=z_0$ and l being the filling length. The dynamic viscosity of the liquid is η, the channel gap thickness is h and θ is the contact angle the liquid makes with the channel walls.

When the viscosity of the displaced fluid is comparable to the liquid viscosity filling the capillary, we use the modified version of Washburn's equation. In equation (4.4), both viscosities affect the filling (in equation (4.3), the small one is neglected):

$$\eta_\alpha \frac{l(t)^2}{2} + \eta_\beta \left(Ll(t) - \frac{l(t)^2}{2} \right) = \left(\frac{\gamma_{lv} h \cos\theta(t)}{6} \right)(t + t_0). \tag{4.4}$$

For fluids having the same viscosity, equation (4.4) reduces to equation (4.5):

$$l(t) = \left(\frac{\gamma_{lv} h \cos\theta(t)}{6\eta_\alpha L} \right)(t + t_0). \tag{4.5}$$

In equations (4.4) and (4.5), t_0 is the integration constant which can be adjusted depending on the initial position of the interface. It is zero if $l(0)$=0. While equation (4.5) scales linearly with time, equation (4.3) scales as ½ power of time as seen in Figure 4.4.

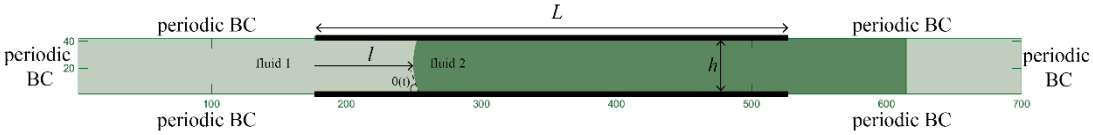

Figure 4.3: Capillary filling problem setup. The wall length is L, the meadow green fluid is liquid and the other one is gas. Filling length (l) is the distance that liquid penetrates into the capillary tube. For the rest of the thesis, the contact angle on black-colored regions on capillary walls is equal to $\theta_{eq} = 60°$.

In Figure 4.3, we show the problem setup. The channel walls of length L are shown in black. The periodic inlet and outlet boundaries ensure mass conservation while the top and bottom periodic sides provide us with a flat interface mimicking infinite reservoirs at both ends. All dimensions are given in lattice units. We use $n_x = 700$ and $n_y = 42$ lattices along x and y-directions, respectively; and place the capillary walls in the middle of the domain at the top and bottom. We set $\kappa = 0.04$, $a = 0.04$

and $M = 1$ in the MRT lattice Boltzmann implementation. Varying M affects the interface velocity [58]. For different viscosity cases we set the kinematic viscosities to $\nu_l = 0.83$ and $\nu_g = 0.067$ (this corresponds to $\tau_\alpha = 3$, $\tau_\beta = 0.7$ as in [58]). The details of the choice of equilibrium distributions etc. are given in Appendix A.

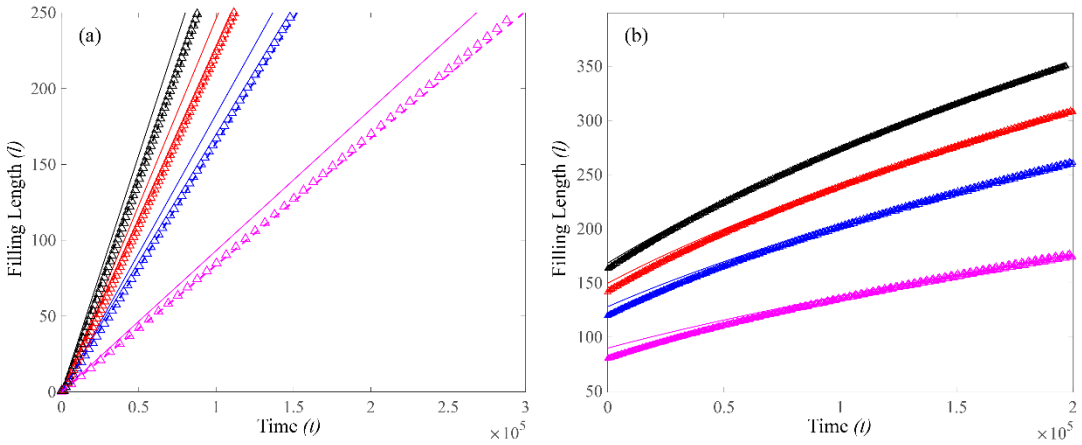

Figure 4.4: The simulation result of filling length as function of time, comparison with Washburn's equation for same (a) and different (b) viscosities. Magenta color is used for $\theta_{eq} = 75°$, blues for $\theta_{eq} = 60°$, reds for $\theta_{eq} = 45°$ and blacks for $\theta_{eq} = 30°$. The symbols are our computations, the solid lines in (a) modified theoretical values for the same viscosity fluids flows (equation 4.5) and in (b) are theoretical values for different viscosity fluids flows (equation 4.3) which are calculated with dynamic angles. The dashed lines in (a) are corrected values for the same viscosity cases.

The differences are, where we observe deviations from initial conditions, Poiseuille flow profile and inertial effects. In Figure 4.4(a), solid lines come from modified Washburn's equation [55] and dashed lines are theoretical values with a refinement of $l^{eff} = l + \frac{h}{2}$. So, we add imaginary walls with a length of $\frac{h}{2}$ at both ends of the capillary tube to get rid of inlet/outlet effects. A similar approach can be seen in Pooley et al. [58]. The filling length data form straight lines because the viscous dissipation occurs in capillary at the same rate. So we observe, it is independent of the interface position. As shown in Figure 4.4(b), after the interface passes the beginning of the capillary, the results agree with Washburn's equation. For the filling distances at a certain time, as we expect, the interface moves faster for lower wetting angles.

Because the capillary driven flow is a contact line motion problem, we also validate if the dynamic contact angles satisfy the Cox-Voinov [70,71] relation which states there is a linear relationship between the cube of dynamic contact angle and the Capillary number.

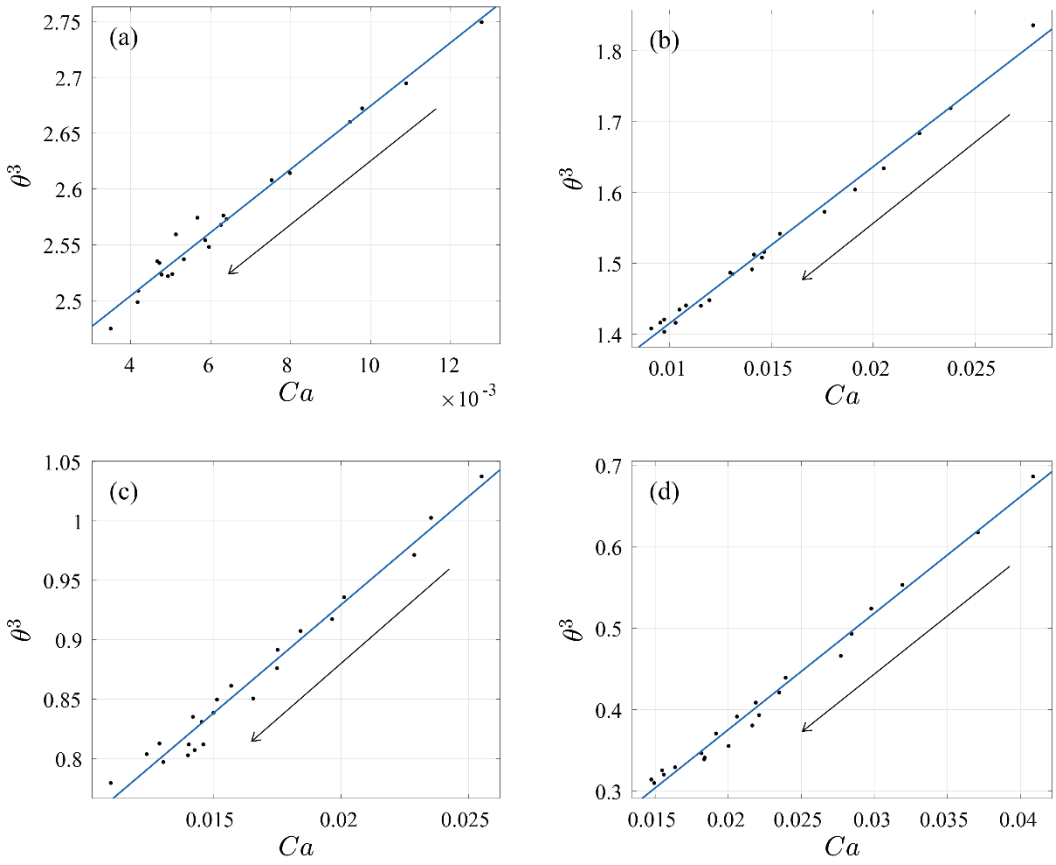

Figure 4.5: Variation of contact angle with Ca, (a) $\theta_{eq} = 75°$, (b) $\theta_{eq} = 60°$, (c) $\theta_{eq} = 45°$, (d) $\theta_{eq} = 30°$, arrows show the filling direction.

We show in Figure 4.5 this linear variation of Ca with the cube of the dynamic contact angle for four different surface energies. Considering each individual case, as the viscosities of the filling and displaced liquids are different, the contact angle of the filling liquid decreases with time and as a result the speed of the filling slows down [72]. But if we compare all cases for different contact angles, speed of the capillary increases with increasing wettability (with lower θ_{eq}) as shown in Figure 4.4.

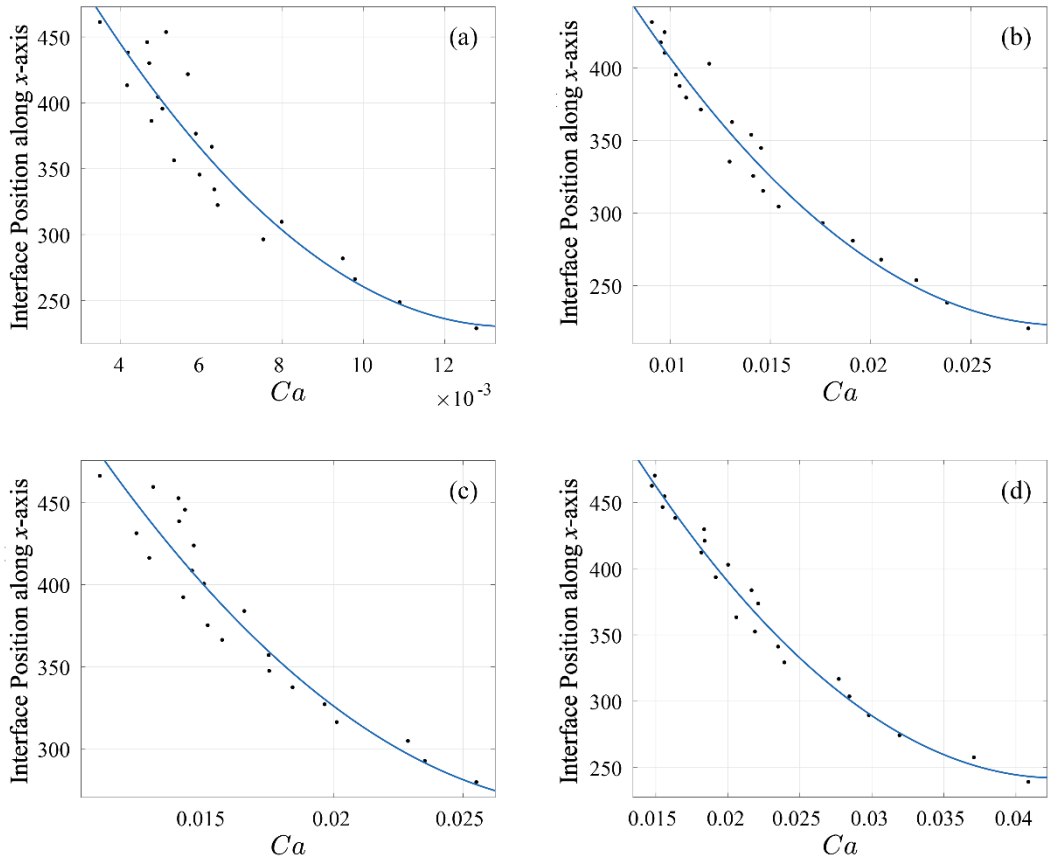

Figure 4.6: Filling length variation with Ca, (a) $\theta_{eq} = 75°$, (b) $\theta_{eq} = 60°$, (c) $\theta_{eq} = 45°$, (d) $\theta_{eq} = 30°$.

For comparison, see the mean velocities (with using Ca values above) for different wettabilities with constant viscosity and surface tension in Figure 4.6.

Apart from these validations, we compare the velocity of the interface with the one given in Figure 4.6 of Pooley and Yeomans [58] and it matches well.

To this end, we validate our solver for both static and dynamic problems.

Chapter 5

Effect of Chemical Heterogeneity

The roughness and chemical heterogeneity are common features of surfaces except the ones manufactured in a laboratory as atomically smooth and chemically homogeneous. Inspired by nature, these features are mimicked to control the motion of interfaces. Among the various micro-fluidic devices, capillary driven flows are popular as there is no need for an external driving mechanism. We study the motion of interfaces in a channel which is driven by capillarity. To slow down or stagnate the interface motion within some regions, we investigate the effects of varying wettability. This can be achieved using electrowetting [73-75] or the channels can be manufactured with chemically and/or physically heterogeneous patterns to pin/depin the interface as a passive control method. We mimic such a surface by chemical heterogeneities on the channel walls.

By chemical heterogeneity we mean the energy of the surface is not uniform, it is altered by modifying the surface chemistry rather than the topology. We achieve this numerically by adjusting the normal gradient of ϕ within the region of interest to achieve the desired θ_{eq}.

Using the channel geometry given in Figure 4.2; we, first, observe the deviation of the interface speed from Washburn's law when there is a chemical defect on the channel walls. To this end, we consider two cases: one with more ($\theta_{eq} = 30°$) and one with less hydrophilic ($\theta_{eq} = 75°$) region on the top wall than the rest of the channel walls which is set to $\theta_{eq} = 60°$. We show this deviation for single defect in Figure 5.1(a) by plotting the time variation of the filling length. We set the length of the defect region to 20 lattices and the deviation from the Washburn's law for $\theta_{eq} = 60°$ everywhere is obvious. The contact line accelerates as it approaches a more hydrophilic area, increasing the filling speed as the slope rises until it passes the area and reaches the regular slope (see squares). The opposite is true for defects that are less hydrophilic. During this region, the contact line motion slows and returns to its

initial speed after (see triangles). We demonstrate the deviation for single patterns on top and bottom walls in overlapping and staggered configurations in panel (b) of the same figure.

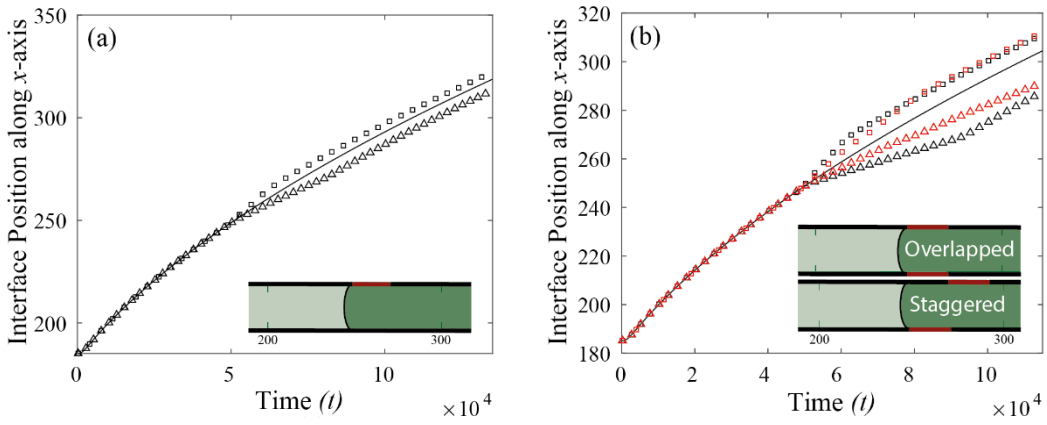

Figure 5.1: The deviation of filling length from Washburn law for $\theta_{eq} = 60°$, with (a) single defect on the capillary (squares for $\theta_{eq} = 30°$and triangles for $\theta_{eq} = 75°$), (b) multi-defects on the capillary (black squares for overlapped $\theta_{eq} = 30°$ regions, black triangles for overlapped $\theta_{eq} = 75°$ regions, red squares for staggered $\theta_{eq} = 30°$ regions and red triangles for staggered $\theta_{eq} = 75°$ regions), to speeds up or down of the interface.

If the patterns are arranged in an overlapped form, the interface motion will slow down more effectively since the contact lines at the top and bottom walls do the same. But, with the staggered configuration, the slowing is constrained since one of the contact lines moves more quickly while the other moves more slowly. We show this in Figure 5.2 by comparing the two configurations. This observation suggest that overlapped heterogeneities prevail over staggered ones to stop the motion of the interfaces.

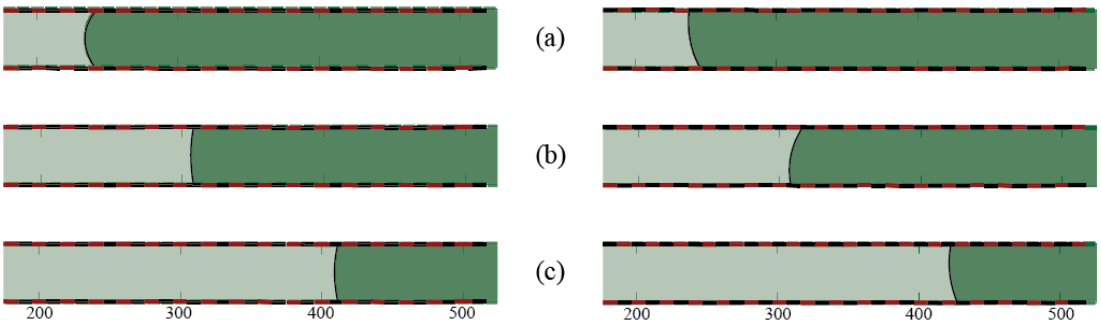

Figure 5.2: Comparison of the effect of wall pattern on the interface motion, the left panel is for the overlapped configuartion while the right panel is for the staggered configuration, (a) t =50000, (b) t =150000, (c) t=400000.

With this motivation, we search for the equilibrium states of the interface; namely, the conditions which flatten the interface resulting in no pressure difference across the interface to derive the motion so that interface stops. In plane, the existence of interface curvature drives the motion. Such a flat interface is possible, for example, if both top and bottom contact angles attain 90°. In the Figure 5.3, we observe a vertical flat interface satisfying our claim. For the top and bottom defects, we set the surface energies for the liquid to have contact angles of 90° while the rest of the channel walls remain at 60°.

Normal stress balance at a local point at the interface with uniform surface tension γ requires

$$p_l - p_g = \gamma \nabla \cdot \boldsymbol{n} \sim \frac{\gamma}{r}, \tag{5.1}$$

where $\boldsymbol{n}$ is the outward unit normal pointing from the liquid into the gas and r is the radius of the curvature of the interface approximated by a circular arc. For the flat case, r goes to infinity and the pressure difference across the interface vanishes. This mechanism stops the interface.

Figure 5.3: Interface of the capillary at 90 degree regions.

But if the regions are staggered not overlapped, then the filling of the capillary may not stop as seen in Figure 5.4. Panels (b) to (e) display the corresponding interface profiles, while panel (a) displays the interface position's deviation from a uniform surface energy surface. The flow slows down but does not stop because $\theta_{eq}^{bot} + \theta_{eq}^{top} < 180°$, it continues to move and only the interface can be flat at the intersection of the regions for a small time interval. Therefore, at that point, the conditions are changed to $\theta_{eq}^{bot} + \theta_{eq}^{top} < 180°$ and the interface again starts to move. Further with time, again the interface becomes symmetric with respect to middle of the domain.

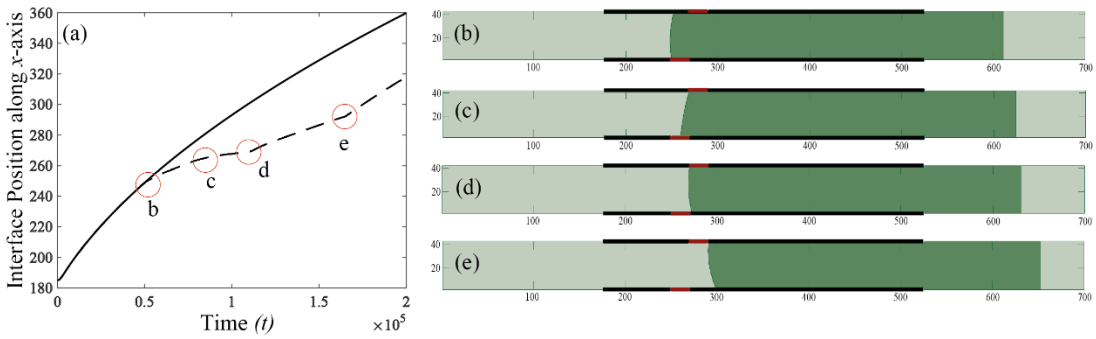

Figure 5.4: History of interface movement for staggered configuration with $\theta_{eq} = 90°$ deffects. The solid line in (a) shows the computed interface position for uniform $\theta_{eq} = 60°$, dashed line is for staggered configuration. The interface shapes at several instants encircled in (a) are shown in panels (b) to (e).

In the Figure 5.5, we see the stopping condition is provided only if $\theta_{eq}^{bot} + \theta_{eq}^{top} \geq 180°$. This means that the flat interface does not have to be vertical. As long as, at any point in time, the contact angles at the top and bottom walls sum up to π, the interface could be stopped even for a staggered configurations with hydrophobic regions.

The use of more hydrophobic regions for overlapped configurations does not affect the stopping mechanism, namely a vertical interface form. But for the staggered

configuration, more hydrophobic regions stop the interface at an inclined position as seen in Figure 5.5.

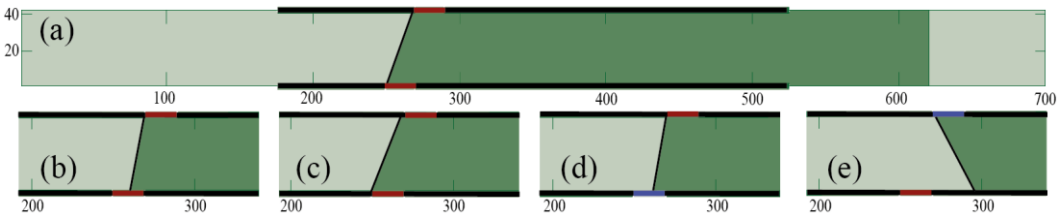

Figure 5.5: Various stopping cases, (a) case 1: Interface of the capillary at 120 degree regions with staggered configuration, (b) case 2, (c) case 3, (d) case 5, (e) case 6; see Table 5.1 for details.

Table 5.1: Stopping conditions using the same setup as in Figure 5.5 for different wettability at defect regions. Except case 7 ($\theta_{eq} = 30°$), all cases have $\theta_{eq} = 60°$ out of the defects.

Parameters and Conditions \ Case Numbers	**Case 1**	**Case 2**	**Case 3**	**Case 4**	**Case 5**	**Case 6**	**Case 7**
$\boldsymbol{\theta_{eq}^{bot}}$ & $\boldsymbol{\theta_{eq}^{top}}$	120&120	100&100	150&150	90&90	100&90	90&120	90&120
Vertically, $\boldsymbol{\theta_{eq}^{bot} + \theta_{eq}^{top} \geq 180°}$	Yes	No	Yes	No	No	2^{nd} region	No
Reaches 2^{nd} region?	No	Yes	No	Yes	Yes	Yes	Yes
Bottom-side contact angle (~%1)	112	100	113	-	100	60	-
Top-side contact angle (~%1)	68	80	67	-	80	120	-
Pinning at 1^{st} or 2^{nd} region?	First	Second	First	-	Second	Second	-
Stopping angle side	Top-side	Bottom-side	Top-side	-	Bottom-side	Bottom-side	-

As we see in the Table 5.1, stopping conditions vary with the wettability of overlapped walls. We define a simple relation between the cases as;

i. If $\theta_{eq}^{bot} + \theta_{eq}^{top} \geq 180°$, the interface stops and the contact line attains the θ_{eq} on the hydrophobic side.
ii. Else, $\theta_{eq}^{bot} + \theta_{eq}^{top} < 180°$, the interface moves but the contact line speed is decreased. When the contact points are on walls that provide $\theta_{eq}^{bot} + \theta_{eq}^{top} \geq 180°$, the interface starts to slow down. It tries to attain θ_{eq} for the side that has already depinned.

We believe that our simulation would motivate further numerical and experimental stuidies for a possible setup for passively driven capillary flows to control the interface motion.

Chapter 6

Motion of Droplets on Wettability Gradient Surfaces

We consider small droplets for which the gravitational forces are negligible and study, in this section, their motion driven by surface energy gradients. To be able to explain the source of this driving mechanism, we, first, define the equilibrium contact angles of droplets on surfaces which do not provide motion. The simplest of such cases is substrates with uniform surface energy around the contact line in equilibrium. This does not require the surface energy be uniform everywhere if there is pinning at a physical roughness. For clean surfaces, the angle contact lines of a droplet makes with the substrate is defined by the Young value. We, here, define the contact angles at the left and right of the center of mass of a droplet as

$$\cos(\theta_e^l) = \frac{\gamma_{SV}^l - \gamma_{SL}^l}{\gamma}, \qquad \cos(\theta_e^r) = \frac{\gamma_{SV}^r - \gamma_{SL}^r}{\gamma}. \tag{6.1}$$

We set the domain length to $n_x = 500$ and height to $n_y = 50$ as seen in Figure 6.1. We initialize the motion by placing the droplet of radius 30 lattice units at $x = 50$ as a semi-circle by using a linear wettability gradient reducing from θ_e^{left} to θ_e^{right}.

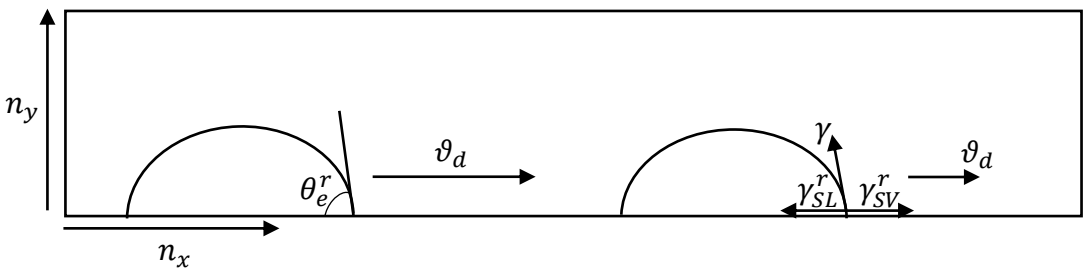

Figure 6.1: Problem set-up for the droplet motion on wettability gradient surface

When the surface energy of the surface the droplet contacts is non-uniform, the contact angles at the two triple junctions are different. If there were any equilibrium state, the angles would be equilibrium angles that we can call as θ_e^l and θ_e^r (as defined in equation (6.1)). The wetting gradient and inequality of the contact angles initates the motion of droplet. Due to hysteresis, it is known that the dynamic angle would be less than the equilibrium angle if the contact line recedes; it would be more if the contact line advances. For a negative wetting gradient surface, the left contact line tries to attain larger contact angle compared to the right contact line. When the left contact line recedes, because the contact angle is smaller than equilibrium angle, the following inequality holds:

$$\gamma_{SV}^l - \gamma_{SL}^l > \gamma \cos(\theta_e^l). \tag{6.2}$$

When the right contact line advances, on the other hand, as the advancing contact angle is larger than the equilibrium contact angle there, the corresponding inequality becomes

$$\gamma_{SV}^r - \gamma_{SL}^r > \gamma \cos(\theta_e^r). \tag{6.3}$$

Summation of the surface tension forces at the two contact lines, then, requires

$$\gamma_{SV}^r - \gamma_{SL}^r - \left(\gamma_{SV}^l - \gamma_{SL}^l\right) > \gamma \left(\cos(\theta_e^r) - \cos(\theta_e^l)\right) > 0 \tag{6.4}$$

for $\theta_e^l > \theta_e^r$, as is the case for negative wetting gradient surface. This generates a net force in positive x-direction which moves the droplet toward right. One could also design a surface with positive wetting gradient and this would drive the motion toward left. In other words, the difference in the contact angles results with a Laplace pressure gradient along the interface, this pressure difference drives the motion.

When the spreading coefficient $S = \gamma_{SV} - \gamma_{SL} - \gamma < 0$, the fluid termed as partial wetting and it can also be defined in terms of the Young value as $S = \gamma(\cos\theta_e - 1)$. For slender droplets, the speed of the droplet on small wetting gradients scales as $\vartheta_d \sim \frac{h_0}{\eta}\frac{dS}{dx} = \frac{h_0\gamma}{\eta}\frac{d\cos\theta_e}{dx} \approx \frac{h_0\gamma}{\eta}\theta_e\frac{d\theta_e}{dx}$ where h_0 is the height and η is the dynamic

viscosity of the droplet, respectively. The driving force explained above is balanced by the viscous stress mostly near the moving contact lines and this balance determines the moving speed [76]. For a droplet moving with constant speed ϑ_d, it scales linearly with $\frac{d\theta_e}{dx}$ for fixed h_0 corresponding to the equilibrium angle $\theta_e(x_0)$ measured at x_0.

In Figure 6.2, we show how the droplet speed varies with wetting gradient (measured in degrees per unit lattice length for different wettability gradient obtained by varying the wetting angle at the left of the domain (θ_e^{left}), as $150°, 135°, 120°, 90°, 60°$, and keeping the one at the right of the domain (θ_e^{right}) fixed at 30°). The droplet moves with a constant speed and we observe a linear relationship between the two for the wetting angles we study: $30° \leq \theta_e \leq 150°$. We should note that, the equilibrium angle approaches 30° toward the end of the domain for all the cases and the theoretical prediciton is valid for small angles.

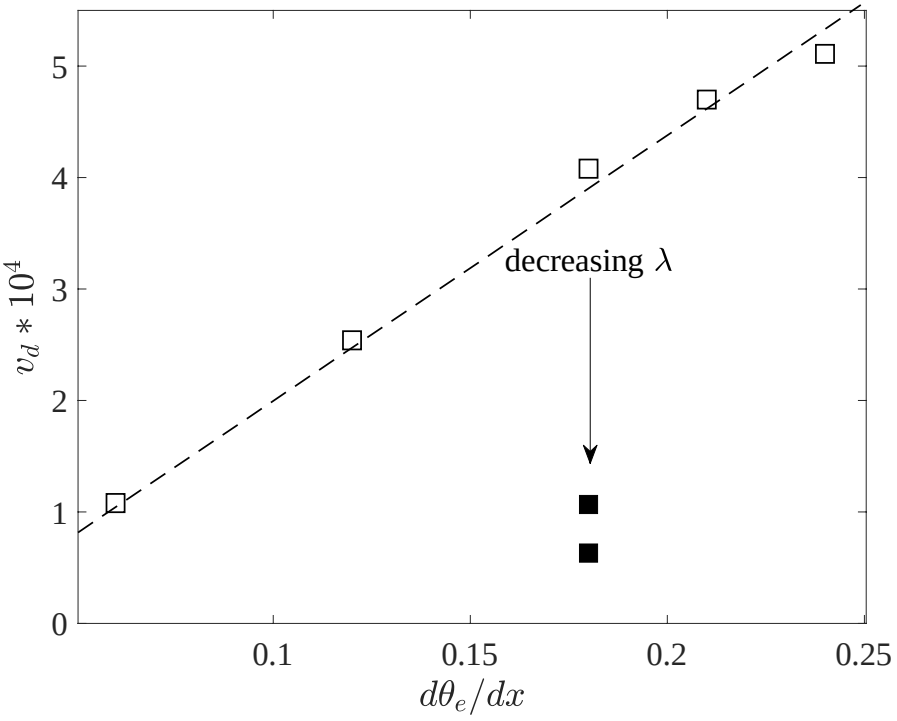

Figure 6.2: Variation of droplet speed as function of wetting gradient. Hollow squares are the terminal speeds for various wetting gradients, dashed line is shown to emphasize the linearity; filled square shows the effect of viscosity ratio.

One would expect, however, the droplet to slow-down if the viscosity of the outside fluid is increased. To show this effect, we study more cases with viscosity ratios of λ=0.1 and 1 on fixed wetting gradient surface, namely 120°-30° case. We show this variation on the same plot with filled squares in Figure 6.2 with a clear observation of slowing down of the droplet if it moves in a viscous fluid.

6.1 Merging of Droplets

Motivated with the simple idea of the previous subsection, we are able to move droplets toward each other and merge. We propose this as a possible use in self-cleaning or water harvesting applications. For example, one could merge small droplets which are able to resist gravity on car shields or windows, merge by the wetting gradient. This would increase the effective bond number [77] of the merged droplet and for sufficiently large volumes, it would move downwards with the aid of gravity. In another example, the merged droplets could be transported directionally depending on the gradients of the wetting patterns on the substrate. We also show that for the merging, the size of the droplet can be different. To this end, we place two droplets on the substrate as shown in Figure 6.3. The gradients are set to be symmetric with respect to $x = x_0$ (mid of the domain) with a gradient of $2 * (\theta_e^l - \theta_e^r)/n_x$. We set n_x and n_y to 250 and 100, respectively, with droplet radii of 30 in lattice units. The history of droplet motion is shown in panels (a) to (d) of Figure 6.3 for equal size droplets. In panels (e) to (h) of the same figure, we show the merging of different size droplets. As can be seen from the velocity vectors (we only show the asymmetric case as it is more intriguing), the outside fluid is squeezed by the motion of the two droplets and leaves the gap at an oblique path due to asymmetry. After the merge, the free surface attains its equilibrium shape; again, at a later time shown in panel (i), we observe the deformation of the interface toward a circular arc; the velocity is maximum at the location where the interface is away from the equilibrium.

To check the influence of viscosity ratio, we change the λ from $0.83/0.067$ to 0.1 and 1. We observe that the droplets slow down due to the increased shear stress on the interface. The droplets move in more viscous fluid, but eventually they merge and attain the same equilibrium shape as in the different viscosity case.

The change in the gradient of the wetting would change the speed, as shown in the previous section, and time for the coalescence; however, it would not affect the idea of merging droplets at a desired location to increase the effective bond number.

This proposition of such wetting gradients used in the merging of droplets further motivates us to stop the motion of a droplet at a desired location. We, finally, postulate that the self-motion of a droplet stops at x_0, with the aid of symmetrically structured gradient walls with respect to the stopping location, x_0.

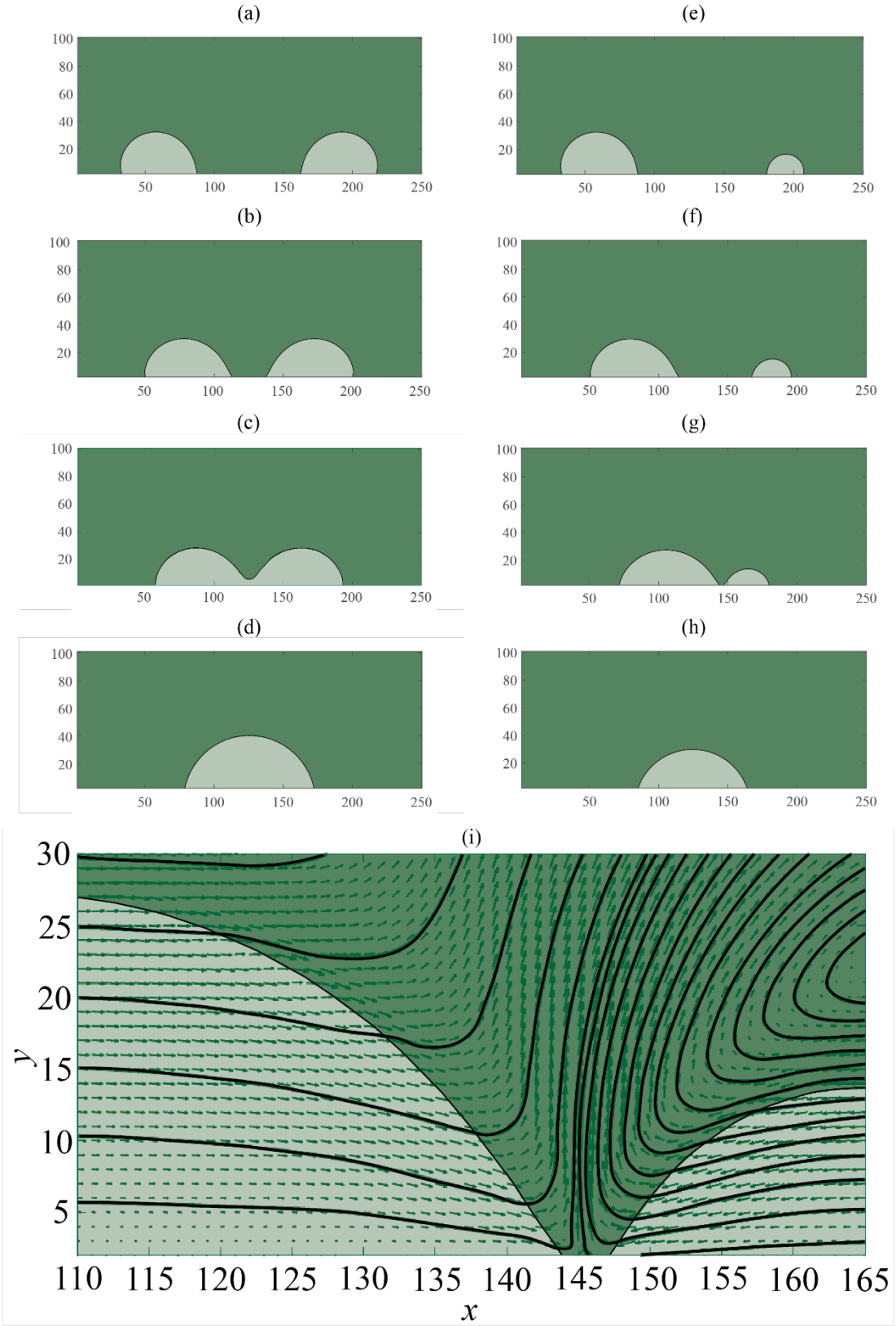

Figure 6.3: The evolution of the merging droplets on wettability gradient surface. (a)-(d) t=5000, 15000, 20000, 50000; (e-h) t=5000, 15000, 30000, 50000; (i) velocity vectors before the different size droplets merge corresponding to (g).

Chapter 7

Confinement Effect

When the droplet is confined from top with a wall as well as bottom, it wets both of the surfaces. For uniform surface energy surfaces, the droplets attain an equilibrium shape which can be called as a fluid column. Because the contact angles of the interfaces are the same at all triple junctions, the shape of the interface becomes a circular arc meeting the walls at the wetting angle. The shape for any contact angle is determined by the geometry. Because the curvature of radius of the interfaces are the same, the pressure jump across the interfaces are the same and there is no pressure difference to drive the column in the confinement. However, generating a wettability gradient surface can trigger the motion.

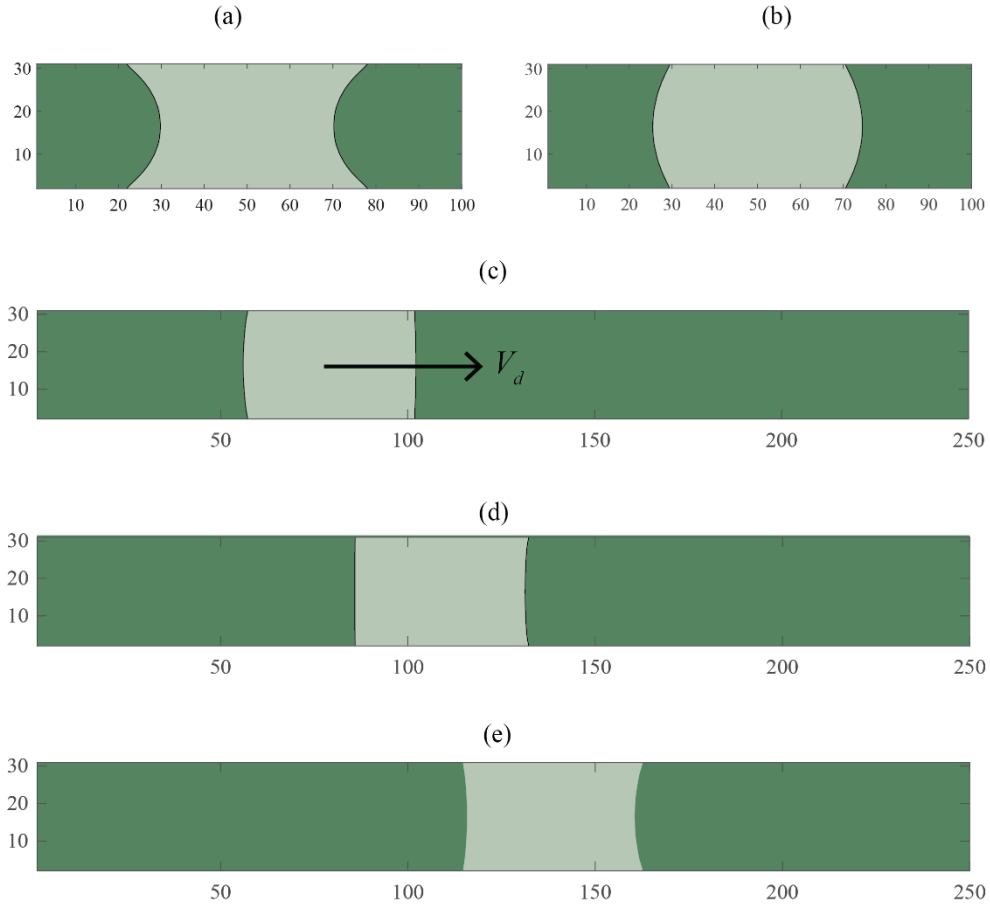

Figure 7.1: The interface profiles for a droplet confined between walls. (a) Equilibrium shape for $\theta_e = 30°$, (b) Equilibrium shape for $\theta_e = 120°$; the motion of liquid column with surface energy gradient (c) *t*=50000, (d) *t*=100000, (e) *t*=150000.

To show this, we first give an equilibrium shape of columns for several surface energies and show the motion if the surfaces designed with surface energy gradient. The same affect is also possible for a wedge shape confinement, but this is a geometric modification for the motion as seen in the self-motion of droplets on conical surfaces and inside wedges (like the self-movement of droplets on cactus spines or liquid columns inside the duck weak).

In Figure 7.1, the two equilibrium shapes obtained for $\theta_e = 30°$ and $\theta_e = 120°$ in panels (a) and (b), wetting and non-wetting columns, respectively. Becuase the surface energies are uniform along the walls; the fluid column cannot move without an external force. The wetting gradient is obtained by setting $d\theta_e/\mathrm{dx}$ to $(\theta_e^l - \theta_e^r)/n_x$ with $\theta_e^l = 120°$, $\theta_e^r = 30$ and $n_x = 250$. This gradient is double of the one

shown in Figure 4.1(a) for 120-30 case and half of the one shown in Figure 6.3. As the viscosity ratio and surface tension between liquid and outside fluid is the same, one would than expect the speed of the column to be twice of the droplet without confinement. The existence of two liquid-solid interfaces doubles the driving force due to hysteresis; however, the viscous losses double as well. Henceforth, the same argument used in Chapter 6 applies. But this time, the pressure difference is not along a single interface: the radius of curvature of the leading interface (though uniform along it) is different than the radius of curvature of the trailing interface (again uniform), this difference generates the Laplace pressure difference from trailing interface to leading interface and this drives the liquid column. The driving mechanisms of single droplet moving on wettability gradient and the one confined look similar but they are different in terms of Laplace pressure.

Chapter 8

Conclusion

In this thesis, we study the interface motion in capillary channels driven by capillary pressure only and self-driven droplets. Apart from the importance of such motions in microfluidic devices as it does not require an external device to drive the motion, it provides us a flow domain to understand and control the interface motion. For this purpose, we modify the surface energy of the channel walls and investigate the passive control mechanism of interfaces instead of active methods.

The problem is investigated by modeling the motion of two-phase flows of Newtonian fluids and integration of the governing equations using MRT lattice Boltzmann Method. This method has many advantages for wetting applications against traditional solvers such as Finite Element Method (FEM) according to computing cost, applicability, mobility between cases etc. We first validate our solver for static and dynamic problems and discuss the effects of surface energy on the motion of interfaces.

We discuss five main problems: (*i*) Accelerating or decelerating the interfaces, (*ii*) interface stopping conditions, (*iii*) self-motion of single droplets on surfaces (*iv*) merging of droplets of same and different size droplets (*v*) self-driven motion of liquid columns within a confinement. According to cases of interface motion driven by capillarity, we can change the contact line speed and stop the interface as needed by playing with the energy of the surfaces. For changing the contact line speed, we add chemical defects on the walls which have different wettability properties. As we expect, according to wettabilities of defects, deviation from the Washburn is observed in Figure 5.1 and for stopping conditions, we show that the defects should provide $\theta_{eq}^{bot} + \theta_{eq}^{top} \geq 180°$ with contact points of interface. The configurations of the defects can change the stopped position of the interface. We explain the

mechanism of the self-motion and show both the effects of gradient and viscosity ratios as well as suggesting several control mechanisms to be used for several applications by directing the motion or stopping the motion of droplets at desired locations or merging them. We also discuss how to self-propel liquid columns confined by walls in a wettability gradient channel otherwise, in uniform surface energy channels, it would stop.

Considering all the problems discussed, we contribute to the understanding and passive control of the interface motion driven by capillarity for further numerical and experimental studies.

References

[1] Wang X, Xu B, Chen Z. Numerical simulation of droplet dynamics on chemically heterogeneous surfaces by lattice boltzmann method. International Journal of Numerical Methods for Heat and Fluid Flow 2020; 30(2): 607–624. doi.org:10.1108/HFF-03-2019-0259

[2] Iwahara D, Shinto H, Miyahara M, Higashitani K. Liquid drops on homogeneous and chemically heterogeneous surfaces: A two dimensional lattice boltzmann study. Langmuir 2003; 19: 9086–9093. doi.org:10.1021/la034456g

[3] Tilehboni SEM, Fattahi E, Afrouzi HH, Farhadi M. Numerical simulation of droplet detachment from solid walls under gravity force using lattice boltzmann method. Journal of Molecular Liquids 2015; 212: 544–556. doi.org:10.1016/j.molliq.2015.10.007

[4] Park CS, Baek SY, Lee KJ. Two-phase flow in a gas injected capillary tube. Advances in Polymer Technology 2003; 22(4): 320–328. doi.org:10.1002/adv.10059

[5] Singh M, Kondaraju S, Bahga SS. Mathematical Model for Dropwise Condensation on a Surface With Wettability Gradient. Journal of Heat Transfer 2018; 140(071502). doi.org:10.1115/1.4039014

[6] Shen C, Liu L, Wu S, Yao F, Zhang C. Lattice Boltzmann simulation of droplet condensation on a surface with wettability gradient. Journal of Mechanical Engineering Science 2020; 234(7): 1403-1413. doi.org:10.1177/0954406219898220

[7] De Gennes PG. Wetting: statics and dynamics. Reviews of Modern Physics 1985; 57(3): 827-863. doi.org:10.1103/RevModPhys.57.827

[8] Marmur A. Contact angle hysteresis on heterogeneous smooth surfaces. J. Colloid Interface Sci. 1994; 168(1): 40–46. doi.org:10.1006/jcis.1994.1391

[9] Marmur A. Thermodynamic aspects of contact angle hysteresis. Advances in Colloid and Interface Science 1994; 50: 121–141. doi.org:10.1016/0001-8686(94)80028-6

[10] Joanny J F, de Gennes P. A model for contact angle hysteresis. J. Chem. Phys. 1984; 81(552). doi.org:10.1063/1.447337

[11] Adamson AW, Gast AP. Physical chemistry of surfaces, 6th ed. A Wiley-Interscience Publication; 1997.

[12] Sonmez I, Cebeci Y. Contact angle hysteresis in a microchannel: Statics. Physical Review Fluids 2019; 4(044008). doi.org:10.1016/j.colsurfa.2003.12.003

[13] Kusumaatmaja H, Yeomans JM. Modeling contact angle hysteresis on chemically patterned and superhydrophobic surfaces. Langmuir 2007; 23(11): 6019–6032. doi.org:10.1021/la063218t

[14] Montes Ruiz-Cabello FJ, Rodriguez-Valverde MA, Marmur A, Cabrerizo V´ılchez MA. Comparison of sessile drop and captive bubble methods on rough homogeneous surfaces: A numerical study. Langmuir 2011; 27(15): 9638–9643. doi.org:10.1021/la201248z

[15] Chang X, Huang H, Lu X, Hou J. Width effect on contact angle hysteresis in a patterned heterogeneous microchannel. J. Fluid Mech. 2022; 949(A15). doi.org:10.1017/jfm.2022.763

[16] Moumen N, Subramanian RS, McLaughlin JB. Experiments on the Motion of Drops on a Horizontal Solid Surface Due to a Wettability Gradient. Langmuir 2016; 22(6): 2682-2690. doi.org:10.1021/la053060x

[17] Raphael E. Spreading of droplets on a patchy surface. C.R. Acad. Sci. Paris II 1988; 306: 751-754.

[18] Xu X, Qian T. Droplet motion in one-component fluids on solid substrates with wettability gradients. Phys. Rev. E. 2012; 85(051601). doi.org:10.1103/PhysRevE.85.051601

[19] Thomas TM, Chowdhury IU, Dhivyaraja K, Mahapatra PS, Pattamatta A, Tiwari MK. Droplet Dynamics on a Wettability Patterned Surface during Spray Impact. Processes 2021; 9(555). doi.org/10.3390/pr9030555

[20] Sadullah MS, Kusumaatmaja H, Launay G, Parle J, Ledesma-Aguilar R, Gizaw Y, *et al*. Bidirectional motion of droplets on gradient liquid infused surfaces. Comm. Phys. 2020; 3(166). doi.org:10.1038/s42005-020-00429-8

[21] Chowdhury IU, Mahapatra PS, Sen AK. Self-driven droplet transport: Effect of wettability gradient and confinement. Physics of Fluids 2019; 31(042111). doi.org:10.1063/1.5088562

[22] Chowdhury IU, Mahapatra PS, Sen AK. Shape evolution of drops on surfaces of different wettability gradients. Chemical Engineering Science 2021; 229(116136). doi.org:10.1016/j.ces.2020.116136

[23] Gulfam R, Chen Y. Recent Growth of Wettability Gradient Surfaces: A Review. A Review Research 2022; 9873075. doi.org:10.34133/2022/9873075

[24] Ding Y, Yin L, Dang C, Liu X, Xu J. Self-climbing of a low surface tension droplet on a vertical conical surface. Colloids and Surfaces A: Physicochemical and Engineering Aspects 2023; 658(130670). doi.org:10.1016/j.colsurfa.2022.130670

[25] Tenjimbayashi M, Manabe K. A review on control of droplet motion based on wettability modulation: principles, design strategies, recent progress, and applications. Science and Technology of Advanced Materials 2022; 23(1): 473-497. doi.org:10.1080/14686996.2022.2116293

[26] Darmanin T, Guittard F. Superhydrophobic and superoleophobic properties in nature. Materials Today 2015; 18(5): 273–285. doi.org:10.1016/j.mattod.2015.01.001

[27] Kohonen MM. Engineered wettability in tree capillaries. Langmuir 2006; 22: 3148–3153. doi.org: 10.1021/la052861x

[28] Barthlott W, Neinhuis C. Purity of the sacred lotus, or escape from contamination in biological surfaces. Planta 1997; 202: 1–8. doi.org:10.1007/s004250050096

[29] Parker AR, Lawrance CR. Water capture by a desert beetle. Nature 2001; 414: 33–34. doi.org:10.1038/35102108

[30] Zheng Y, Gao X, Jiang L. Directional adhesion of superhydrophobic butterfly wings. Soft Matter 2007; 3: 178–182. doi.org: 10.1039/B612667G

[31] Yager P, Edwards T, Elain F, Helton K, Nelson K, Tam MR, *et al*. Microfluidic diagnostic technologies for global public health. Nature 2006; 442: 412–418. doi.org:10.1038/nature05064

[32] Sackmann EK, Fulton AL, Beebe DJ. The present and future role of microfluidics in biomedical research. Nature 2014; 507: 181–189. doi.org:10.1038/nature13118

[33] Yeo LY, Chang HC, Chan PPY, Friend JR. Microfluidic devices for bioapplications. Small 2011; 7(1): 12–48. doi.org:10.1002/smll.201000946

[34] Wu L, Guo Z, Liu W. Surface behaviors of droplet manipulation in microfluidics devices. Advances in Colloid and Interface Science 2022; 308(102770). doi.org:10.1016/j.cis.2022.102770

[35] Oliveira NM, Vilabril S, Oliveira MB, Reis RL, Mano JF. Recent advances on open fluidic systems for biomedical applications: A review. Mater. Sci. Eng. C. Mater. Biol. Appl. 2018; 97: 851-863. doi.org:10.1016/j.msec.2018.12.040

[36] Gosh A, Ganguly R, Schutzius TM, Megaridis CM. Wettability patterning for high-rate, pumpless fluid transport on open, non-planar microfluidic platforms. Lab. Chip 2014; 14: 1538-1550. doi.org:10.1039/C3LC51406D

[37] Hassan G, Yilbas BS, Al-Sharafi A, Al-Qahtani H. Self-cleaning of a hydrophobic surface by a rolling water droplet. Sci. Rep. 2019; 9(5744). doi.org:10.1038/s41598-019-42318-3

[38] Sonmez I, Cebeci Y. Investigation of relationship between critical surface tension of wetting and oil agglomeration recovery of barite. Colloids and Surfaces A: Physicochem. Eng. Aspects 2004; 234: 27–33. doi.org:10.1016/j.colsurfa.2003.12.003

[39] Dupuis A, Yeomans JM. Lattice boltzmann modelling of droplets on chemically heterogeneous surfaces. Future Generation Computer Systems 2004; 20: 993–1001. doi.org:10.1016/j.future.2003.12.012

[40] Léopoldés J, Dupuis A, Bucknall DG, Yeomans JM. Jetting micronscale droplets onto chemically heterogeneous surfaces. Langmuir 2003; 19: 9818–9822. doi.org:10.1021/la0353069

[41] Verberg R, Pooley CM, Yeomans JM, Balazs AC. Pattern formation in binary fluids confined between rough, chemically heterogeneous surfaces. Physical Review Letters 2004; 93(18). doi.org:10.1103/PhysRevLett.93.184501

[42] Au AK, Lai H, Utela BR, Folch A. Microvalves and micropumps for biomems. Micromachines 2011; 2(2): 179–220. doi.org:10.3390/mi2020179

[43] Hilber W. Stimulus-active polymer actuators for next-generation microfluidic devices. Applied Physics A 2016; 122(751). doi.org:10.1007/s00339-016-0258-6

[44] Arango Y, Temiz Y, Gokce O, Delamarche E. Electro-actuated valves and self-vented channels enable programmable flow control and monitoring in capillary-driven microfluidics. Science Advances 2020; 6(16). doi.org:10.1126/sciadv.aay8305

[45] Mahmud MS, Alo A, Farshchian B, Lee GH, Kim N. Pulsed laser ablation on polymethylmethacrylate (pmma) surfaces for capillary driven flows. Surfaces and Interfaces 2022; 31(101989). doi.org:10.1016/j.surfin.2022.101989

[46] Mistura G, Pierno M. Drop mobility on chemically heterogeneous and lubricant-impregnated surfaces. Adv. in Phys.: X 2017; 2: 591-607. doi.org:10.1080/23746149.2017.1336940

[47] Daniel S, Chaudhury MK, Chen JC. Fast Drop Movements Resulting from the Phase Change on a Gradient Surface. Science 2001: 291: 633-636. doi.org:10.1126/science.291.5504.633

[48] Chen L, Gao M, Liang J, Wang D, Hao L, Zhang L. Lattice Boltzmann simulation of wetting gradient accelerating droplets merging and shedding on a circumferential surface. Eng. App. of Comp. Fluid Mech. 2022; 16. doi.org:10.1080/19942060.2022.2116488

[49] Qu J, Yang X, Wang Z. Numerical simulations on the self-motion of droplets in hydrophobic microchannels driven by wettability gradient surfaces. Int. Comm. in Heat and Mass Trans. 2020; 119(104961). doi.org:10.1016/j.icheatmasstransfer.2020.104961

[50] Li C, Dai H, Gao C, Wang T, Dong Z, Jiang L. Bioinspired inner microstructured tube controlled capillary rise. PNAS 2019; 116(26): 12704-12709. doi.org:10.1073/pnas.1821493116

[51] Chapman S, Cowling TG. The mathematical theory of non-uniform gases, 3rd ed. Cambridge Mathematical Library; 1970.

[52] Dutka F, Napiorkowski M, Dietrich S. Mesoscopic analysis of gibbs' criterion for sessile nanodroplets on trapezoidal substrates. The Journal of Chemical Physics 2012; 136(064702). doi.org:10.1063/1.3682775

[53] Kusumaatmaja H, Pooley CM, Girardo S, Pisignano D, Yeomans JM. Capillary filling in patterned channels. Physical Review E 2008; 77(067301). doi.org:10.1103/PhysRevE.77.067301

[54] Zhao J, Chen S, Liu Y. Droplets motion on chemically/topographically heterogeneous surfaces. Molecular Simulation 2016; 42: 1452–1459. doi.org:10.1080/08927022.2016.1198478

[55] Kusumaatmaja H. Lattice boltzmann studies of wetting and spreading on patterned surfaces (doctoral thesis). Oxford: University of Oxford; 2008.

[56] Zhang J, Li B, Kwok DY. Metastable contact angles and selfpropelled drop movement on chemically , heterogeneous surfaces by a meanfield lattice boltzmann model. Eur. Phys. J. Special Topics 2009; 171: 73–79. doi.org:10.1140/epjst/e2009-01013-y

[57] Krüger T, Kusumaatmaja H, Kuzmin A, Shardt O, Silva G, Viggen EM. The lattice boltzmann method: Principle and practice, 1st ed. Springer; 2017. 407–431.

[58] Pooley CM, Kusumaatmaja H, Yeomans JM. Modelling capillary filling dynamics using lattice boltzmann simulations. Eur. Phys. J. Special Topics 2009; 171: 63–71. doi.org:10.1140/epjst/e2009-01012-0

[59] Kendon VM, Cates ME, Pagonabarraga I, Desplat JC, Bladon P. Inertial effects in three dimensional spinodal decomposition of a symmetric binary fluid mixture: a lattice boltzmann study. J. Fluid Mech 2001; 440: 147–203. doi.org:10.1017/S0022112001004682

[60] Bray A. Theory of phase-ordering kinetics. Advances in Physics 1994; 43(3): 357–459. doi.org:10.1080/00018739400101505

[61] Swift MR, Orlandini E, Osborn WR and Yeomans, JM. Lattice boltzmann simulations of liquid-gas and binary fluid systems. Physical Review E. 1996; 54(5): 5041–5052. doi.org:10.1103/physreve.54.5041

[62] Briant AJ, Yeomans JM. Lattice boltzmann simulations of contact line motion. ii. binary fluids. Physical Review E 2004; 69(031603). doi.org:10.1103/PhysRevE.69.031603

[63] Pooley CM, Kusumaatmaja H, Yeomans JM. Contact line dynamics in binary lattice boltzmann simulations. Physical Review E 2008; 78(056709). doi.org:10.1103/PhysRevE.78.056709

[64] Krüger T, Kusumaatmaja H, Kuzmin A, Shardt O, Silva G, Viggen EM. The lattice boltzmann method: Principle and practice, 1st ed. Springer; 2017. 65–66.

[65] Bhatnagar PL, Gross EP, Krook M. A model for collision processes in gases. I. small amplitude processes in charged and neutral one component systems. Physical Review 1954; 94(3): 511–525. doi.org:10.1103/physrev.94.511

[66] Zou Q, He X. On pressure and velocity boundary conditions for the lattice Boltzmann BGK model. Phys. Fluids 1997; 9(6): 1591-1598. doi.org:10.1063/1.869307

[67] Ladd A. Numerical simulations of particulate suspensions via a discretized boltzmann equation. part 1. theoretical foundation. Journal of Fluid Mechanics 1994; 271: 285-309. doi.org:10.1017/s0022112094001771

[68] Schrader M. Young-dupre revisited. Langmuir 1995; 11: 3585–3589. doi.org:10.1021/la00009a049

[69] Washburn EW. The dynamics of capillary flow. The Physical Review 1921; 17(3): 273-283. doi.org:10.1103/PhysRev.17.273

[70] Cox R. The dynamics of the spreading of liquids on a solid surface. part 1. viscous flow. Journal of Fluid Mechanics 1986; 168(1): 169–194. doi.org:10.1017/s0022112086000332

[71] Voinov O. Hydrodynamics of wetting. Fluid Dynamics 1977; 11(5): 714-721. doi.org:10.1007/bf01012963

[72] Latva-Kokko M, Rothman DH. Scaling of dynamic contact angles in a lattice-boltzmann model. Physical Review Letters 2007; 98(254503). doi.org:10.1103/PhysRevLett.98.254503

[73] Teng P, Tian D, Fu H, Wang S. Recent progress of electrowetting for droplet manipulation: from wetting to superwetting systems. Mater. Chem. Front. 2020; 4(140). doi.org:10.1039/c9qm00458k

[74] Olanrewaju A, Beaugrand M, Yafia M, Juncker D. Capillary microfluidics in microchannels: from microfluidic networks to capillaric circuits. Lab. Chip. 2018; 18(16): 2323–2347. doi.org:10.1039/c8lc00458g

[75] Mugele F, Klinger A, Buehrle J, Steinhauser D, Herminghaus S. Electrowetting: a convenient way to switchable wettability patterns. J. Phys.: Condens. Matter 2005; 17: 559–576. doi.org:10.1088/0953-8984/17/9/016

[76] Broachard F. Motions of Droplets on Solid Surfaces Induced by Chemical or Thermal Gradients. Langmuir 1989; 5(2): 432-438. doi.org:10.1021/la00086a025

[77] Ceyhan U, Tiktas A, Ozdogan M. Pinning and depinning of Wenzel-state droplets around inclined steps. Colloid and Interface Science Communications 2020; 35(100238). doi.org:10.1016/j.colcom.2020.100238

Appendices

Appendix A

The Choice of Equilibrium Distribution

Based on minimizing the magnitude of spurious velocities close to interfaces, we present the optimal equilibrium distributions and stencils for computing spatial derivatives for the lattice Boltzmann algorithm [63] as

$$f_i^{eq}(\boldsymbol{r}) = \frac{w_i}{c^2}\left(p_0 - \kappa\emptyset\nabla^2\emptyset + e_{i\alpha}\rho u_\alpha + \frac{3}{2c^2}\left[e_{i\alpha}e_{i\beta} - \frac{c^2}{3}\delta_{\alpha\beta}\right]\rho u_\alpha u_\beta\right) + \frac{\kappa}{c^2}\left(w_i^{xx}\partial_x\emptyset\partial_x\emptyset + w_i^{yy}\partial_y\emptyset\partial_y\emptyset + w_i^{xy}\partial_x\emptyset\partial_y\emptyset\right), \tag{A.1}$$

$$g_i^{eq}(\boldsymbol{r}) = \frac{w_i}{c^2}\left(\Gamma\mu + e_{i\alpha}\emptyset u_\alpha + \frac{3}{2c^2}\left[e_{i\alpha}e_{i\beta} - \frac{c^2}{3}\delta_{\alpha\beta}\right]\emptyset u_\alpha u_\beta\right), \tag{A.2}$$

for $i = 1, \dots, 8$,where $w_{1-4} = \frac{1}{3}$, $w_{5-8} = \frac{1}{12}$ and twice appearing indices mean summation over those indices. Other parameters are $w_{1-2}^{xx} = w_{3-4}^{yy} = \frac{1}{3}$, $w_{3-4}^{xx} = w_{1-2}^{yy} = -\frac{1}{6}$, $w_{5-8}^{xx} = w_{5-8}^{yy} = -\frac{1}{24}$, $w_{1-4}^{xy} = 0$, $w_{5-6}^{xy} = \frac{1}{4}$ and $w_{7-8}^{xy} = -\frac{1}{4}$.

When $i = 0$, stationary values are selected to maintain the concentration of each species,

$$f_0^{eq}(\boldsymbol{r}) = \rho - \sum_{i=1}^{8} f_i^{eq}(\boldsymbol{r}), \qquad g_0^{eq}(\boldsymbol{r}) = \emptyset - \sum_{i=1}^{8} g_i^{eq}(\boldsymbol{r}). \tag{A.3}$$

Derivatives and the Laplacian terms are calculated with using stencils,

$$\bar{\partial}_x = \frac{1}{12\Delta x}\begin{bmatrix} -1 & 0 & 1 \\ -4 & 0 & 4 \\ -1 & 0 & 1 \end{bmatrix}, \quad \bar{\nabla}^2 = \frac{1}{6(\Delta x)^2}\begin{bmatrix} 1 & 4 & 1 \\ 4 & -20 & 4 \\ 1 & 4 & 1 \end{bmatrix}. \tag{A.4}$$